Chapter 10

Laboratory Tests on Dynamic Properties of Soils

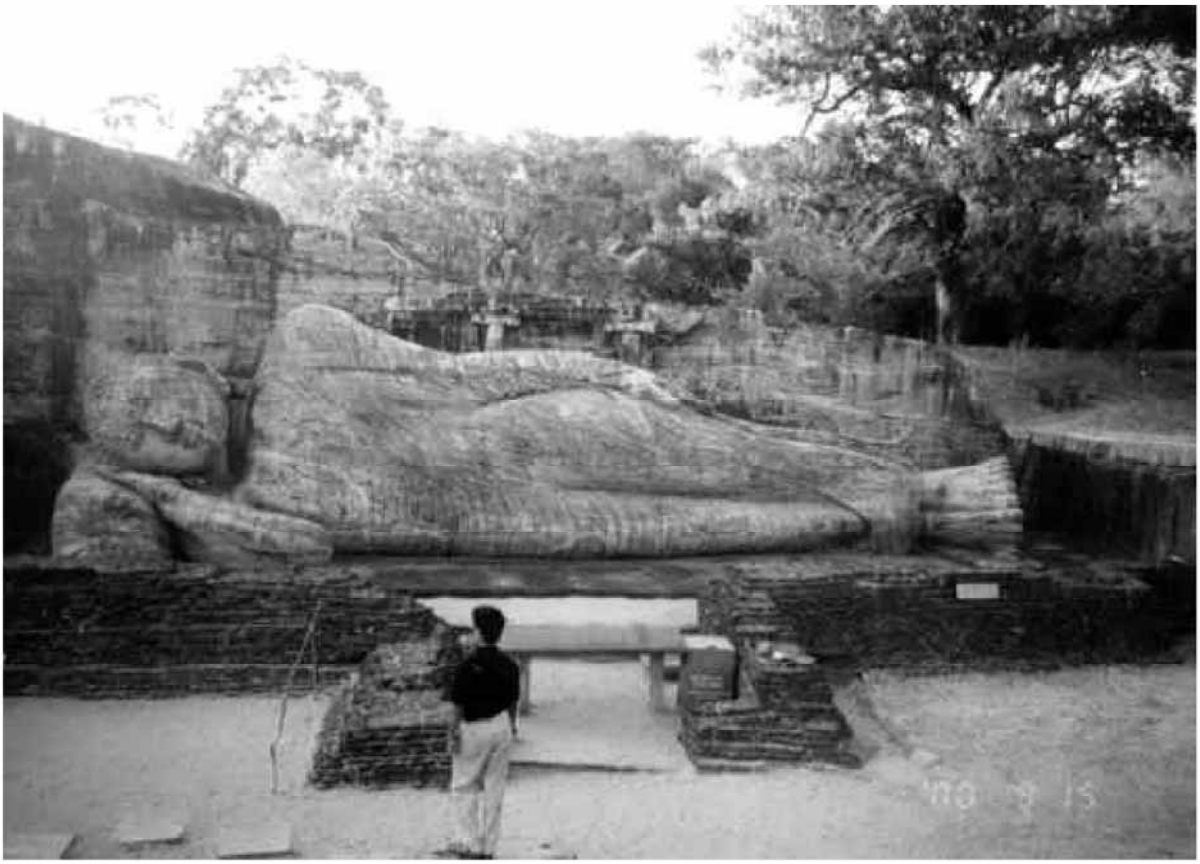

Nirvana, the dying shape of Buddha in Boronnaruwa, Sri Lanka.
Bhuddism in its earliest stage was accepted in Sri Lanka and was then transferred to South East Asia.
A legend states that Bhuddha's mother came down from the heaven to see him after his death, and Bhudda revived for a short time.

10.1 Resonant Column Tests of Soils

Laboratory testing skills have been needed to determine G/G_{max} and h in a small strain range of 10^{-6}–10^{-2} (0.0001%–1%). It was, however, difficult in 1960s and 70s to precisely measure the stress–strain behavior in the small strain range (<10^{-4} approximately). The solution to this problem was the resonant column test (共振法試験).

The method of resonant column test was developed by K. Iida in 1930s. It became popular worldwide since 1950s. Firstly, Ishimoto and Iida (1936, 1937) developed both a theory and a device for resonant column tests on soils, in which the loading frequency at the maximum response was employed to determine elastic properties of soils. Since no confining pressure was able to be applied to consolidate specimens at their times, soil samples with fines and moisture, that could maintain shape without pressure application, were tested. Later, Iida (1938) carried out tests on dry sand which was supported by cellophane sheets. Since no effective stress was applied in these tests, the measured V_s, ranging from V_s = 50 m/s to V_s = 200 m/s, appears to be low.

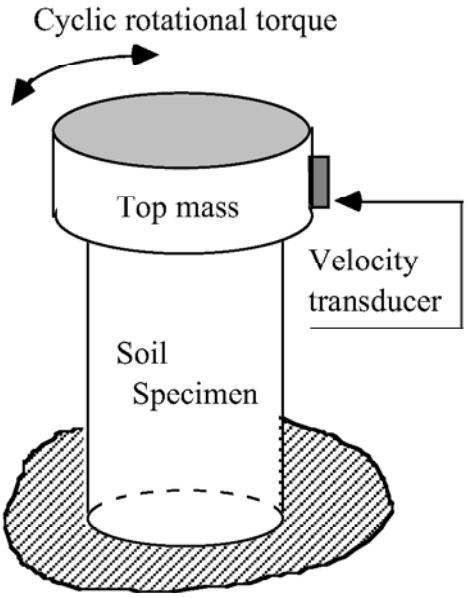

Fig. 10.1 Cylindrical specimen undergoing resonant column test

This testing technique applies cyclic force to a soil specimen at various frequencies. The dynamic response of a specimen to this force is measured in terms of velocity and/or acceleration. While a precise measurement of small displacement (deformation) is difficult, velocity and acceleration at a high frequency are large enough to be measured. By varying the loading frequency, the variation of amplification in amplitude of response is plotted against the frequency. Fig. 10.1 illustrates the testing method conceptually and Fig. 10.2 is an idea of test results.

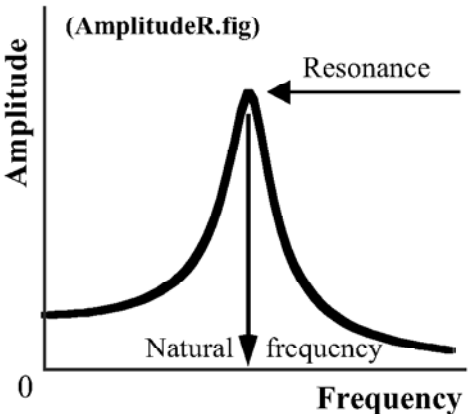

Fig. 10.2 Interpretation of resonant column test

The soil specimen in Fig. 10.1 is fixed at the bottom and is subjected to torsion at the top. By applying the idea of wave propagation to torsion of a solid cylinder with a top mass, a theoretical value of resonant (natural) frequency is detected. By equating the theoretical and experimental resonant frequencies (Fig. 10.2), the shear modulus, G, is obtained.

For example, when there is no top mass in Fig. 10.1, the natural period of soil column, T_n, in torsional shear is given by

$$T_n = 4H/V_s$$

When the resonance or the maximum response occurs at the loading frequency of T_n^* (or the frequency of $1/T_n^*$) in the test, this experimental value and the theoretical value are equated. Hence,

$$T_n^* = 4H/V_s,\quad V_s = \sqrt{G/\rho} = 4H/T_n^*,\ \text{and}\ \ G = \rho\left(4H/T_n^*\right)^2.$$

The shear strain in a specimen (= top displacement/specimen height) varies in the radial direction: zero at the center and maximum at the perimeter (円周). Hence, the average value is employed in interpretation.

The damping ratio is obtained by using the logarithmic decrement (Fig. 9.8) or the maximum response of $1/(2h)$ or $1/\sqrt{2}$ of amplification (Sect. 9.4). It is noteworthy that resonant column tests give G and h after repeating more number of cycles of loading than what occurs in most earthquake events.

One of the limitations of resonant column tests is the number of loading cycles that a soil specimen experiences during tests. Since the number is significantly greater than that in real earthquakes, the obtained modulus and damping ratio correspond to those after many cycles. Note that earthquakes of magnitude = 7 or less have only a few significant shaking cycles (see Fig. 5.6 and Table 19.1). Another shortcoming is that resonant column tests on water saturated specimens under large strain amplitudes cause liquefaction (Ellis et al. 2000). This is because high frequency shaking makes free drainage of pore water impossible.

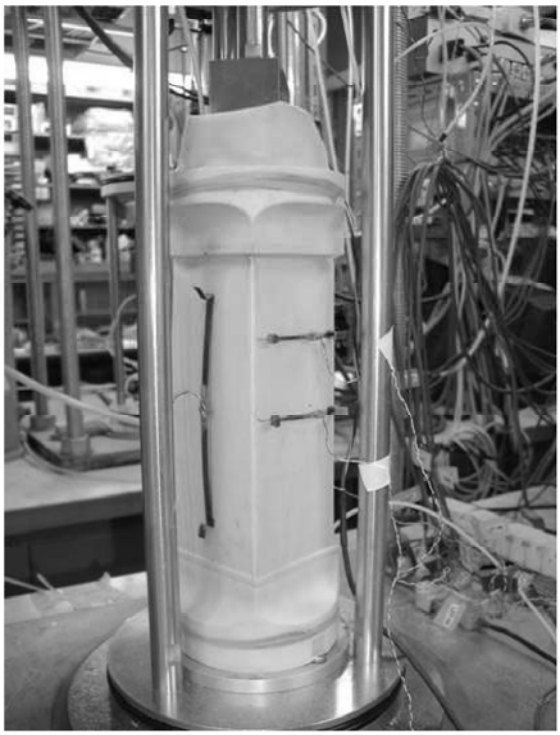

Fig. 10.3 Local displacement transducer attached on triaxial shear specimen

Recent developments in laboratory testing technique have made resonant column tests less important than before. This is because stress–strain data at small strain amplitude can be precisely measured today, which was impossible in and before 1970s. For example, a local displacement transducer (LDT) in Fig. 10.3 is able to record a very small displacement of 0.25 μm (Goto et al. 1991). This sensitivity is equivalent with strain of 1.25×10^{-6} for a sample size of 20 cm.

10.2 General Principle in Interpretation of Strain Amplitude Effects on Shear Modulus and Damping Ratio

In 1970s and early 80s a plenty of experimental studies were made of nonlinearity of soil undergoing cyclic loading. They are summarized and presented in this chapter. It will be shown therein that such factors as particle size, effective stress level, plasticity of clays, and many others affect the variation of shear modulus and damping ratio with the strain amplitude. Since there are so many studies made so far, they may cause confusion among readers. To avoid this situation, one basic principle that governs the nonlinearity is briefly described in this section.

Shear modulus of an ideally elastic material is never affected by the strain amplitude. Damping ratio of an elastic material is null. This is an extreme situation on one hand. On the other hand, sand and, in particular, gravelly soils have a significant nonlinearity; shear modulus and damping ratio change with the strain amplitude. It is inferred therefore that the extent of nonlinearity varies with the discreteness of the concerned material. Discreteness means how the constituent particles of soil are separated from one another. This idea is schematically illustrated in Fig. 10.4 and Fig. 10.5. In more details,

1. In sand and gravels without fines, particles are not bonded. They simply maintain contact and friction. This situation is called highly discrete. Test results on sand and gravel, which will be presented later, exhibit more significant nonlinearity than those on clay (Sect. 10.6).
2. Moreover, the magnitude of effective stress in sand and gravel affects the nonlinearity. Higher stress generates more interaction among grains and reduces the discreteness. Consequently, the nonlinearity decreases. Conversely, sand and gravel under lower effective stress exhibit more nonlinearity. See Sects. 10.6 and 10.8.
3. Clays with greater plasticity index (*PI=LL–PL* in Sect. 1.1) have more connection among grains than less plastic clays. This connection is generated not only by the grain-to-grain contact forces (effective stress) but also by the increased electric and chemical interactions. Thus, more plastic clays are not so discrete as less plastic clays and sands. Consequently, the nonlinearity of plastic clays is not so significant as compared with other kinds of soils (Sects. 10.6 and 10.13).

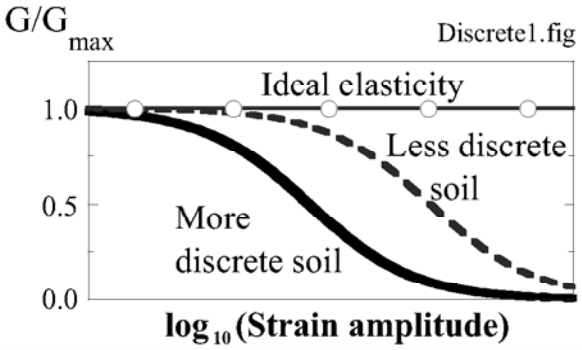

Fig. 10.4 Effects of discreteness of soils on nonlinearity in terms of variation of shear modulus with strain amplitude

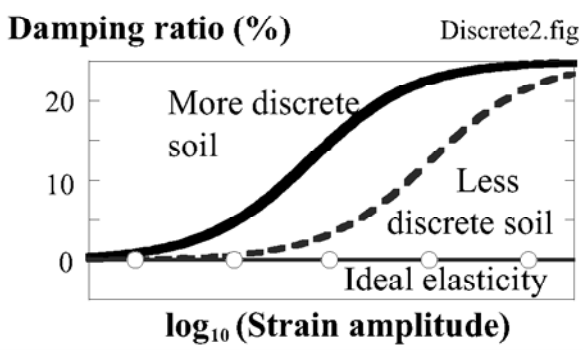

Fig. 10.5 Effects of discreteness of soils on nonlinearity in terms of variation of damping ratio with strain amplitude

10.3 Factors That Affect Modulus and Damping of Sand

There are many test results that studied the cyclic deformation of soils. It is known today that the following factors affect the shear modulus and damping ratio.

For shear modulus of sandy soils, first,

(1) strain amplitude, (2) effective stress, (3) density or void ratio, and (4) anisotropic consolidation.

On the contrary, the degree of overconsolidation (overconsolidation ratio, OCR) does not significantly affect the shear modulus of sand. The effects of grain size is less important. For details, see the following sections.

The damping ratio of sand varies with

(1) strain amplitude and (2) effective stress level.

Damping ratio of soil is independent of loading frequency (Sect. 10.9). Therefore, laboratory test to determine damping of sand can be carried out at a relatively low frequency (e.g., 0.1 Hz) by using a pneumatic-controlled device. This device is cheaper than hydraulic ones that can work at such a higher frequency as encountered during earthquakes. Further, void ratio and anisotropic consolidation do not significantly affect damping ratio of sand. Overconsolidation is not important either.

Cyclic drained test on Toyoura sand in Fig. 10.6 shows that modulus increases and energy damping (area of stress–strain loop) decreases with the number of cycles. Although the effective stress and the isotropic consolidation state did not change with the number of cycles and the void ratio decreased only slightly, the modulus and damping varied drastically. Because such a variation is often encountered during laboratory testing, most reported G and h come from the 10th or 15th cycles. Accordingly, those reported values may not be appropriate for the first few cycles or analysis on earthquakes of smaller magnitude (less number of cycles). Note that resonant column tests (Sect. 10.1) report values after thousands of cycles of loading.

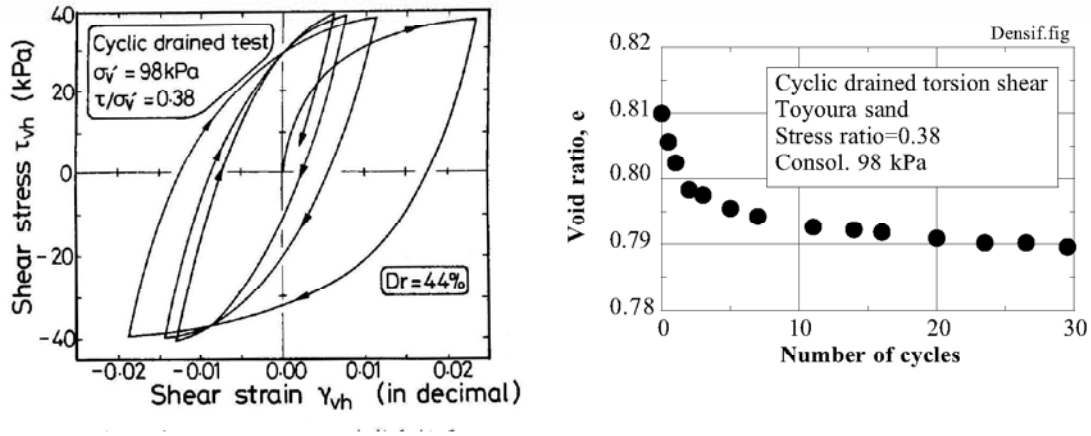

Fig. 10.6 Cyclic deformation of sand in drained test (Towhata et al. 1985)

Difference between sand and clay

Sand and clay are called cohesionless and cohesive soils. They are different in the following points.

1. Particle size of clay is much smaller than the size of sand grains. This smaller grain size makes water seepage more difficult in clay.
2. Clay particles have electric charges. They can attract water around them. Therefore, the water content of clay can be high. When compressed, consequently, clay reveals large consolidation settlement.
3. Cemented sand has bonding between grains. But, bonding that develops with age is more significant in clay. Cohesion that is the shear strength under zero effective stress is a product of bonding.

Secant shear modulus of clay (Fig. 10.7) is affected by

(1) strain amplitude, (2) density or void ratio or water content (when saturated with water), (3) effective stress, (4) overconsolidation, (5) consolidation time, and (6) prestraining (previous cyclic loading). Among these, (1)–(3) are more important.

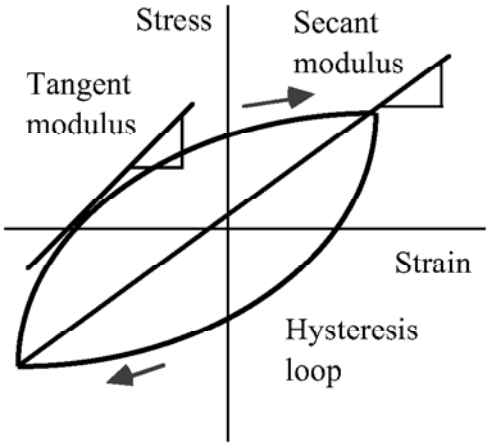

Fig. 10.7 Definition of secant and tangent shear moduli

Shear modulus of clay is not much affected by loading frequency (Sect. 6.1). It is affected by strain amplitude.

Damping ratio of clay is not affected by

(1) loading frequency and (2) effective stress. The effects of consolidation time seems less important.

Similar to sand, the modulus and damping ratio of clay vary with the number of loading cycles. Figure 10.8 compares the stress–strain loops that were observed during the first and the tenth cycles of loading. In contrast to sand that underwent drained cyclic loading and became stiffer with the number of cycles (Sect. 10.3), clay in Fig. 10.8 became softer with the number of cycles. This seems to be because

- excess pore water pressure increased and consequently the effective stress decreased with the number of cycles, reducing the frictional resistance between clay grains, and
- bonding between grains were destroyed and clay became softer.

The second mechanism is widely experienced during determination of sensitivity by unconfined compression tests (一軸圧縮試験による鋭敏比の決定).

The softening of clay during cyclic loading (Fig. 10.8 and Fig. 10.9) is called degradation. This is important in the problem of offshore platforms subjected to storm-wave loading. Note that storm loading exerts thousands of cycles of loading that is much greater than the number of cycles included in earthquake motions.

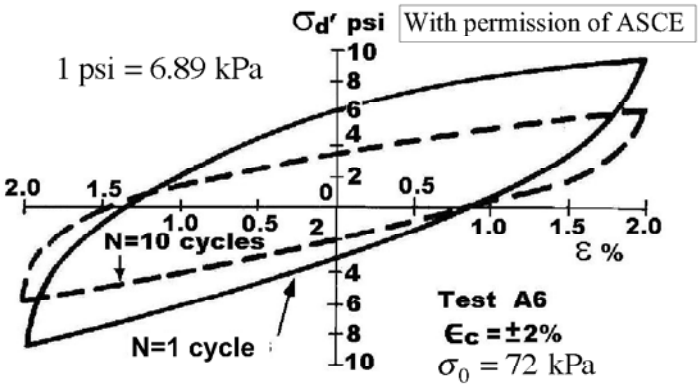

Fig. 10.8 Hysteresis loops measured during first and tenth cycles (Idriss et al. 1978)

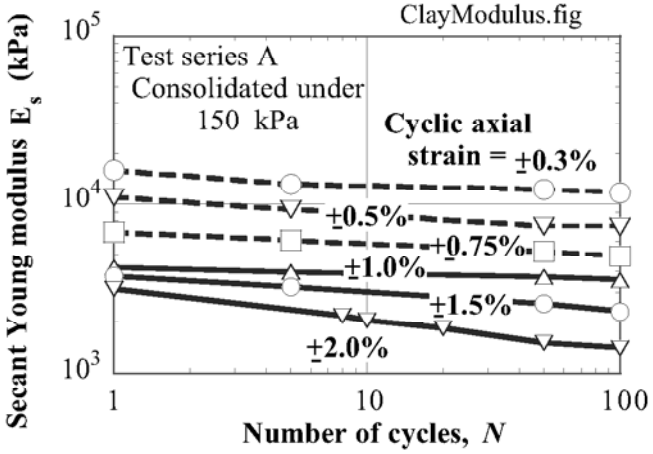

Fig. 10.9 Variation of secant modulus with number of cycles in clay (drawn after Idriss et al. 1978)

10.5 Shear Modulus of Sand at Small Strain Amplitude

The shear modulus, $G = G_{max}$, at small strain amplitude, which is typically 10^{-6} (=0.0001%) or less, is considered as one of the basic soil parameters. This modulus is most adequately determined from shear wave velocity (V_s), which is measured directly in-situ (原位置観測); $V_s = \sqrt{G_{max}/\rho}$. When this is not possible, a use of SPT-*N* (*N*値; for example, see Sect. 8.4) is commonly practiced. Field investigation on V_s or *N* is not possible when a studied earth structure is not yet constructed. This is a case of a planned dam and a planned land reclamation. Then, a study of dynamic response of a planned structure requires V_s or G_{max} to be determined by the following methods:

1. Disturbed soil specimen is collected at a borrow area and consolidated in a laboratory at a planned density (土取場で乱した土を採取し、実験室で所要の密度で圧密する). Cyclic tests are run on reconstituted specimens (実験室で調製された試料) and "shear modulus *G*" as well as "*h*" is determined over a range of strain amplitude. *G* at a very small strain gives G_{max}.
2. Use is made of an empirical formula such as

$$G_{max} = 700\frac{(2.17-e)^2}{1+e}(P')^{0.5} \quad (\text{kgf/cm}^2) \quad \text{(for round sand)}$$

$$G_{max} = 330\frac{(2.97-e)^2}{1+e}(P')^{0.5} \quad (\text{kgf/cm}^2) \quad \text{(for angular sand)}$$

by Richart et al. (1970) in which "*e*" stands for the void ratio of sand and the effective mean principal stress of P′ is defined by $P' = (\sigma_1' + \sigma_2' + \sigma_3')/3$. Noteworthy is that empirical formulae do not care the specific nature of a concerned soil. It should be used only for preliminary purposes.

kgf = kg as force
1 kgf/cm^2 = 98 kN/m^2
= 98 kPa

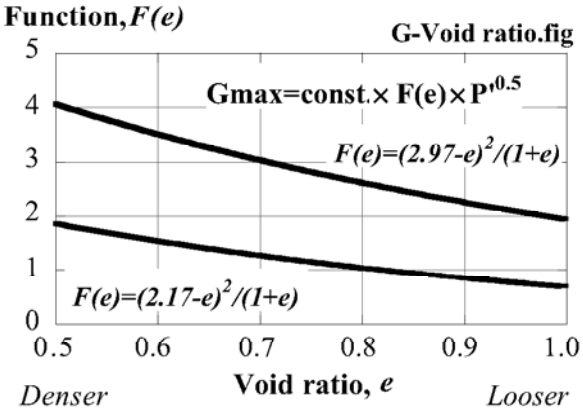

Fig. 10.10 Empirical relationship between void ratio and shear modulus, G_{max}

The formulae shown above indicate two important points:

- The effects of void ratio on shear modulus are taken into account by an empirical function of $F(e) = (2.17–e)^2/(1+e)$ or $(2.97–e)^2/(1+e)$. Since denser sand has a greater value of modulus, $F(e)$ increases as "*e*" decreases (see Fig. 10.10).
- Shear modulus increases in proportion to the square root of the effective stress. In a level ground, $P' = \frac{1+2K_o}{3}\sigma_v'$, where K_o is the lateral earth pressure coefficient and σ_v' is the effective vertical stress. Accordingly, $V_s = \sqrt{G_{max}/\rho}$ increases in proportion to $(P')^{1/4}$.
- Constant parameters of 700 and 330 stand for the effects of all other factors. They are nothing but average values of data from many types of sand. Hence, they may not be appropriate for any specified sand.
- At such a very small strain amplitude as 10^{-6} (0.0001%), any soil is said to be elastic. Hence, G_{max} at such a small strain amplitude seems to be an elastic shear modulus. There may be no hysteresis loop, making h = 0%. There is an opinion, however, that there is a small damping ratio such as h = 2% even at a very small strain amplitude. Otherwise, there may be an infinite amplification at a resonance frequency of subsoil, which is not very realistic.

Deformation modulus (*G* or *E*) of soil at small strain is determined by two different ways in laboratories. One is the measurement of wave propagation velocity (Fig. 10.11; $G_{max} = \rho V_s^2$ for example). The obtained modulus is called dynamic modulus. The other method is the very precise laboratory measurement of stress and strain in soil samples (Fig. 10.3). The modulus thus obtained is called static modulus.

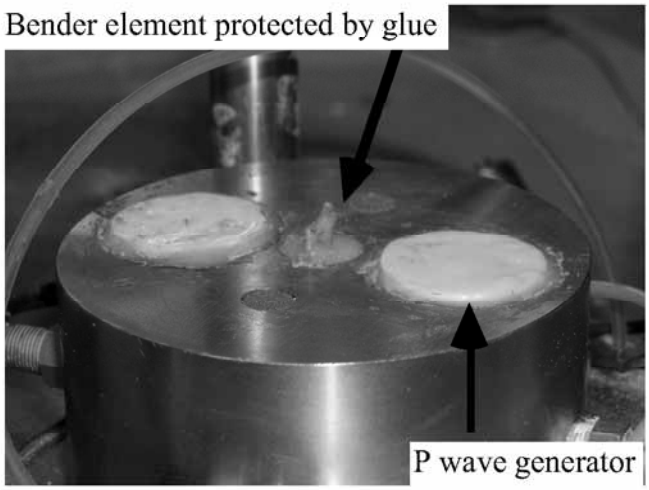

Fig. 10.11 Bender element attached to bottom of triaxial device

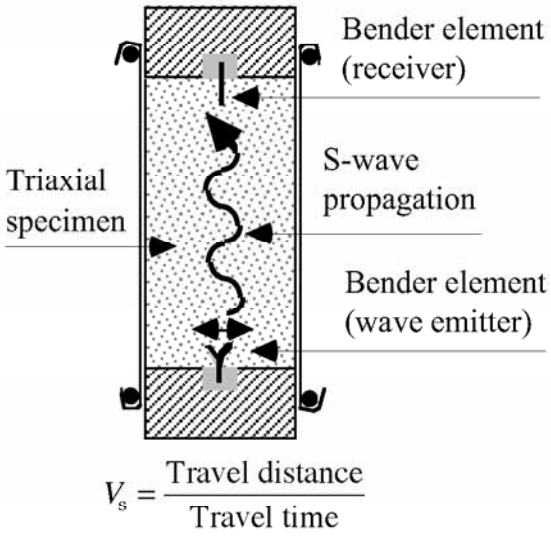

Fig. 10.12 Measurement of wave propagation velocity by bender elements

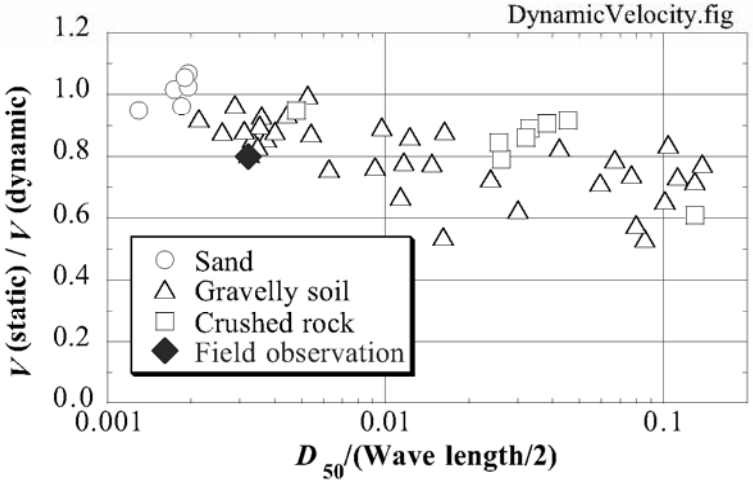

Fig. 10.13 Comparison of dynamic and static moduli at small strain (data by Tanaka et al. 2000 and Maqbool and Koseki, 2006)

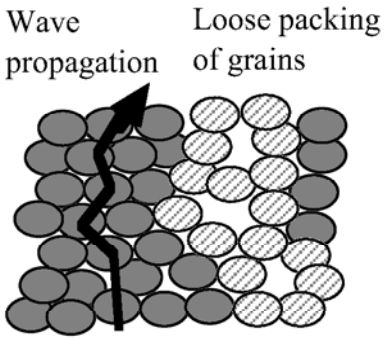

Fig. 10.14 Different mechanisms of dynamic and static moduli

A bender element in Fig. 10.11 is a device that shakes at high frequencies in the horizontal direction and generates S-wave propagation from one end towards the other end of a soil specimen (Fig. 10.12). The S-wave velocity is determined by using the travel distance and the travel time (Viggiani and Atkinson, 1995). In spite of this simple concept, there are some uncertainties. First, it is not clear whether the travel distance is the distance between two ends of the sample, the distance between tips of bender elements, or else. Moreover, the travel time is supposed to be the time difference between wave emission and wave arrival. The wave arrival cannot be clearly defined. The arrival of initial shaking or the arrival of the peak give different times. This uncertainty is because the wave field is not one-dimensional but is subjected to more complicated near-field effects (Brignoli et al. 1996). For P-wave generation, a piezo electric device is available.

Conceptually, the small strain moduli should be identical whether measured dynamically or statically. In reality, however, the dynamic modulus is greater than the static modulus as shown in Fig. 10.13 in which experimental and field data by Tanaka et al. (2000) and Maqbool and Koseki (2007) are illustrated. Note that data of both V_p and V_s are plotted together in this figure. Although two kinds of modulus (wave velocity) are similar in fine sand (small grain size, D_{50}), the wave velocity as calculated from static modulus ($\sqrt{G_{max}/\rho}$) becomes smaller than the dynamically measured wave velocity (static modulus <

dynamic modulus) as the grain size becomes greater.

The main reason for the difference between two moduli is probably that wave propagates along rigid particles and the obtained modulus stands for the rigidity of stable grain packing, while the static modulus represents the overall deformation of a soil specimen and is affected particularly by loose and soft parts in it. This point is conceptually demonstrated in Fig. 10.14.

At small strain ($<10^{-5}$), a stress–strain loop is reduced to a nearly straight line: an elastic behavior. The secant modulus of $G = \tau/\gamma$ decreases as the strain amplitude increases. It is a convention to study separately the effects of strain-nonlinearity from such factors as the effective stress and density:

$$G = G_{max}(\textit{function of } \sigma',\ e,\ \text{etc.}) \times (G/G_{max}). \tag{10.1}$$

Thus, the effect of strain is indicated by G/G_{max}.

G_{max} is frequently designated by G_o. Fig. 10.15 (Kokusho, 1987) compares G/G_{max} measured on laboratory-reconstituted samples of clean sand under *drained* conditions. The importance of undrained shear tests on undisturbed samples will be discussed in Sect. 10.17. Since G varies with the number of cycles (Sect. 10.3), the data in Fig. 10.15 shows G in the 10th–20th cycles. Figure 10.15 indicates the following:

1. G/G_{max} decreases as the strain amplitude increases
2. The reduction of G/G_{max} is less significant when the effective stress is higher
3. Nevertheless, most sands exhibit similar G/G_{max} curves irrespective of different testing conditions

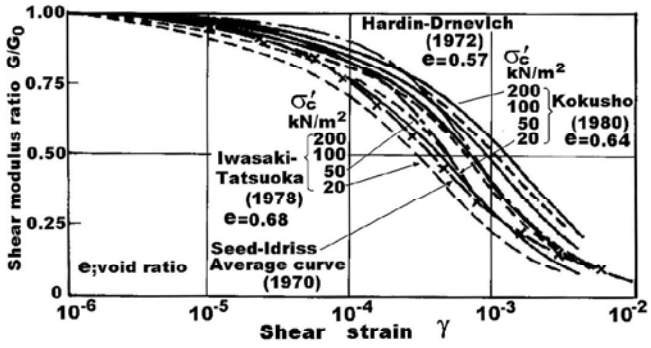

Fig. 10.15 G/G_{max} of reconstituted clean sands (Kokusho, 1987)

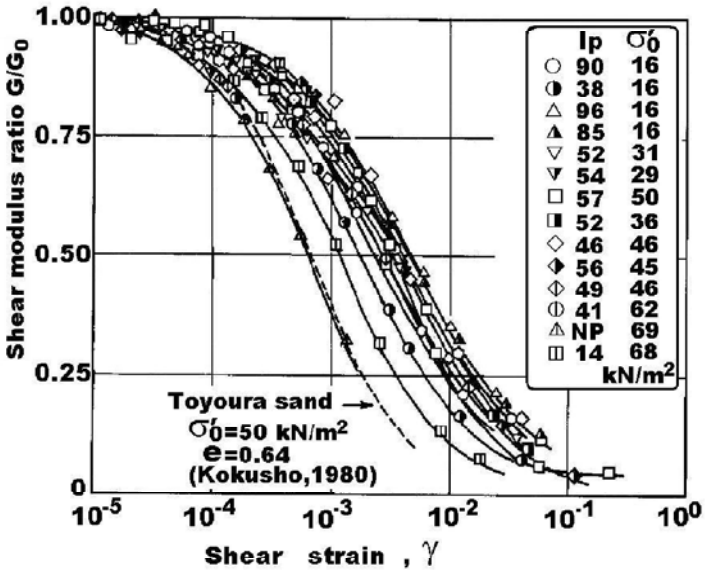

Fig. 10.16 G/G_{max} of clays with different I_p (Kokusho, 1987)

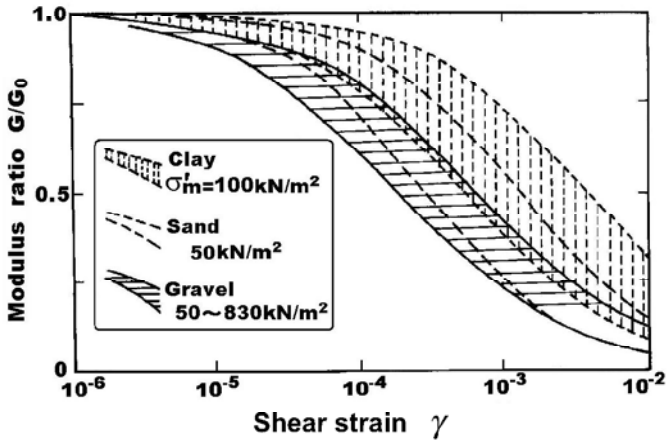

Fig. 10.17 Effects of soil type on G/G_{max} (summary made by Imazu and Fukutake, 1986)

Figure 10.16 shows data obtained from cohesive soils. It may be seen that those soils with larger I_p (plasticity index, Sect. 1.1) indicate greater G/G_{max}, suggesting that a greater cohesion keeps G/G_{max} large up to a large strain amplitude. Kokusho (1987) then quoted a summary of many data by Imazu and Fukutake (1986) to confirm this point. Figure 10.17 clearly indicates that G/G_{max} is greater for clay and smaller for sand and gravel.

It should be noted therefore that the effects of strain amplitude (i.e., decrease in G/G_{max}) is more significant when the soil grains are separated or discrete from each other more substantially. Discreteness is the case when grains have no cohesion and when the effective stress is low.

The amplitude of strain stands for the single amplitude. When the shear strain varies between $-\gamma_a$ and γ_a, the single amplitude is γ_a. The double amplitude stands for $2\times\gamma_a$.

10.7 Effects of Effective Stress on Shear Modulus of Sand

Figure 10.15 already showed that G/G_{max} is affected by the effective stress to some extent. However, the more important effects of the effective stress occurs in G_{max} at small strain amplitude.

Chung et al. (1984) carried out resonant column tests (see Sect. 10.1) on clean sand. Their specimens were isotropically consolidated under an effective stress of σ_3'. The following natures of resonant column tests should be borne in mind:

1. Test is possible in relatively small strain range
2. The number of loading cycles prior to measurement is very large; possibly thousands
3. The loading frequency is high, being of order of 100 Hz

Figure 10.18 indicates the variation of G with the strain amplitude between 10^{-4} and 10^{-1} % (from 10^{-6}–10^{-3} in decimal). The higher effective stress is associated with the greater shear modulus.

Figure 10.19 illustrates the variation of G_{max} with the effective stress. This figure shows that

1. G_{max} increases in proportion to $\sigma_3'^{0.5}$
2. The effects of void ratio, e, on G_{max} is approximated by an empirical formula of $(2.97-e)^2/(1+e)$

It is a common practice today in equivalent-linear dynamic analyses to

1. First, determine G_{max} at small strain amplitude by running in-situ tests (downhole survey etc.) or by using a rough empirical formula by means of SPT-N: $V_s = 80N^{1/3}$ for sand (Sect. 8.4)
2. Second, find out an appropriate G/G_{max} vs. γ correlation
3. Finally, $G = G_{max} \times (G/G_{max})$ gives the shear modulus at any strain amplitude

This practice means that G_{max} takes into account site-specific conditions: type of soil, the effective stress, age, over-consolidation, fines content, etc., while G/G_{max} is rather independent of those factors as repeatedly shown in this chapter.

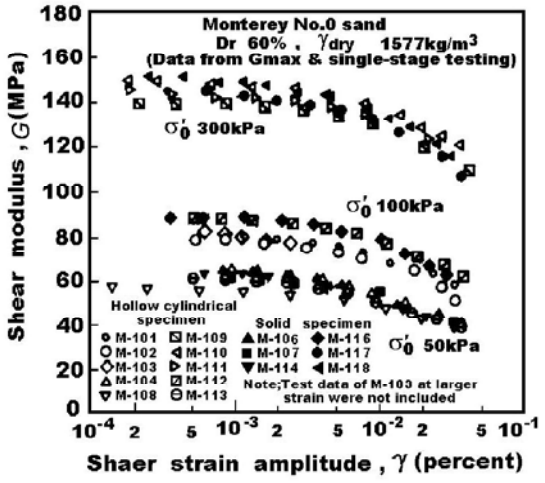

Fig. 10.18 Effects of effective stress on G (Chung et al. 1984)

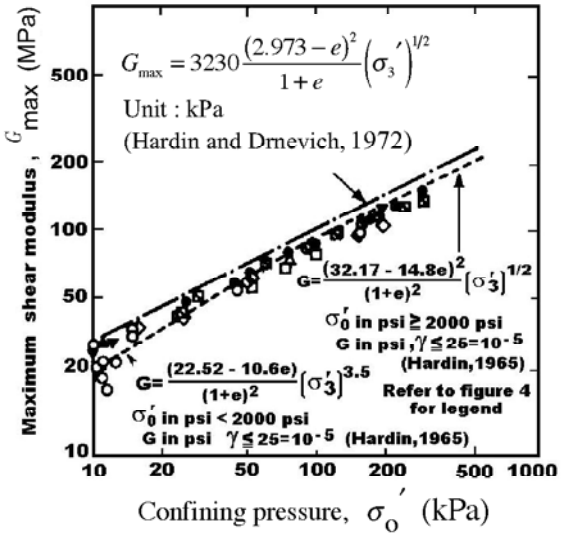

Fig. 10.19 Variation of G_{max} with effective stress (drawn after Chung et al. 1984)

As was shown in Sect. 10.3, the shape of a hysteresis stress–strain loop of sand undergoing drained cyclic shear changes with the number of loading cycles. The secant shear modulus increases with the cycles while the area of loops decreases. Consequently, the damping ratio decreases with the progress of the cyclic loading. Therefore, most laboratory tests report the damping ratio in the 10th–20th cycles without paying attention to the first few cycles.

Figure 10.20 by Kokusho (1987) indicates the effects of soil type on damping ratio. Since sand and gravel have a greater damping ratio than clay, it may be said that the more discrete material has the greater energy damping than more continuous soils.

The damping ratio of sand in Fig. 10.20, however, is larger than that for gravel probably because the sand was tested under lower effective stress (50 kPa). If correction is made for this point, the damping ratio of sand will be smaller than that for gravel.

The resonant column tests by Chung et al. (1984) indicate the influence of the effective stress level on damping ratio of sand. Figure 10.21 compares three series of tests that were conducted under the effective stress of 50, 100, and 300 kPa. The damping ratio is greater when the pressure is lower. This observation is consistent with the idea in Sect. 10.6 that G decreases more rapidly under lower pressures, indicating a more nonlinear behavior.

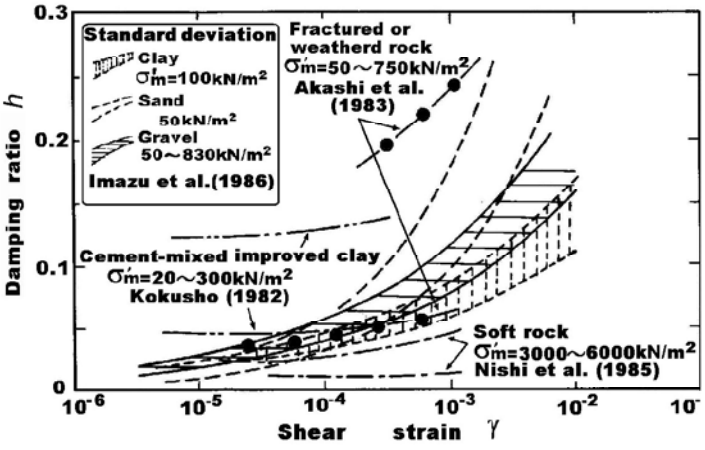

Fig. 10.20 Damping ratio of different types of soils (Kokusho, 1987)

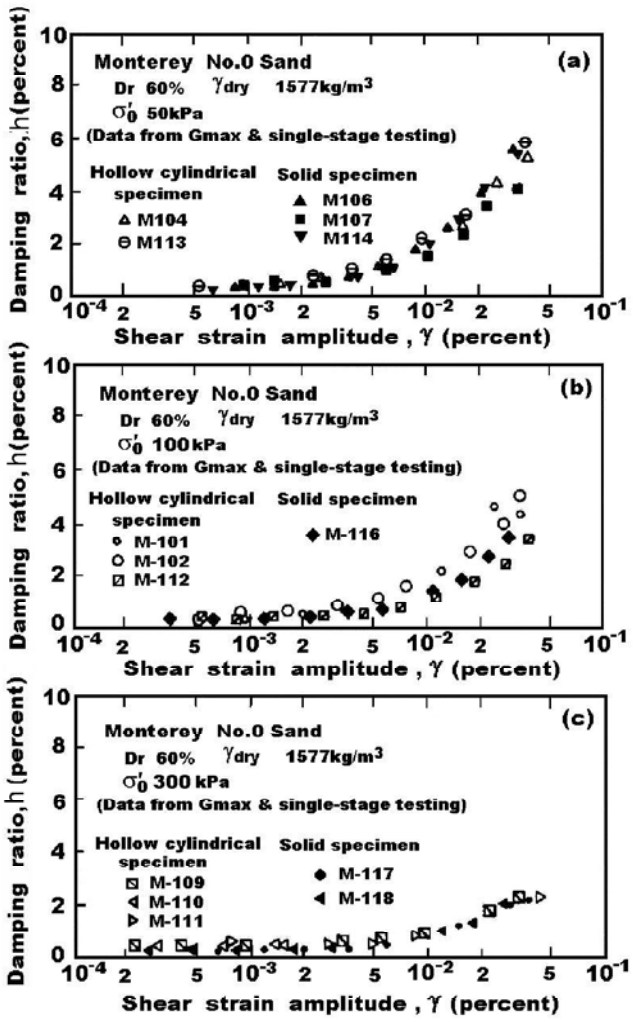

Fig. 10.21 Damping ratio of different effective stress level (Chung et al. 1984)

The energy damping described here may not account for all the energy dissipation. A recent discussion is made of wave reflection inside a sandy layer. The heterogeneous V_s in sandy layer due to increase of the effective stress in the vertical direction causes complex transmission and reflection and disperses the wave energy. Much is not known about this effects.

This section addresses the effects of loading rate on the stress–strain behavior of clay. Casagrande and Shannon (1948a,b) performed unconfined compression tests on clays at different speeds. The rate of strain varied thousands of times and in case of remoulded kaolinite, the peak strength increased about 70% (Fig. 10.22). Lefebvre and LeBoeuf (1987) conducted monotonic shear tests on clay to find greater rigidity and strength when the rate of loading was faster.

One of the difficulties in testing clays is the drainage condition and heterogeneous deformation of a specimen. Since the permeability is low in clay, the nonuniformity in strain induces different excess pore water pressure in a specimen, making the stress–strain behavior dependent on the nonuniformity. This problem appears to be more significant when the rate of loading is faster, because the excess pore water pressure has even a shorter and less sufficient time to adjust the nonuniform pressure distribution.

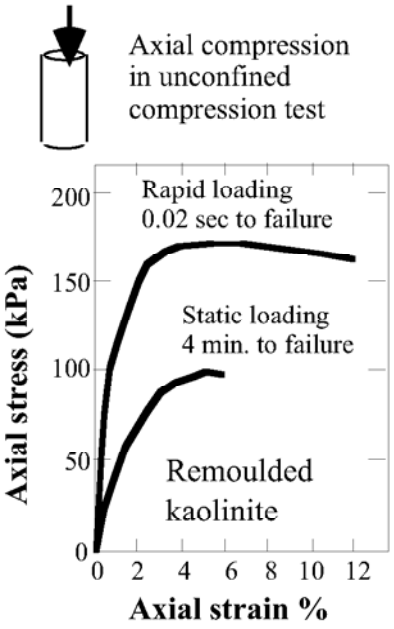

Fig. 10.22 Effects of loading rate on shear deformation of clay (Casagrande and Shannon, 1948a)

Hara (1973) conducted cyclic loading on a variety of clays. His strain amplitude seems relatively small. His results in Fig. 10.23 do not suggest significant rate dependency.

Kokusho (1982) presents in Fig. 10.24 the effects of loading frequency on G and damping ratio of clay. It seems that G increases with the increase of frequency. The damping ratio is larger under lower frequency than under higher frequency. According to constant-volume cyclic tests, which is equivalent with undrained shear, by Lefebvre and Pfendler (1996), 12% increase in strength occurred per one log cycle of rate of deformation.

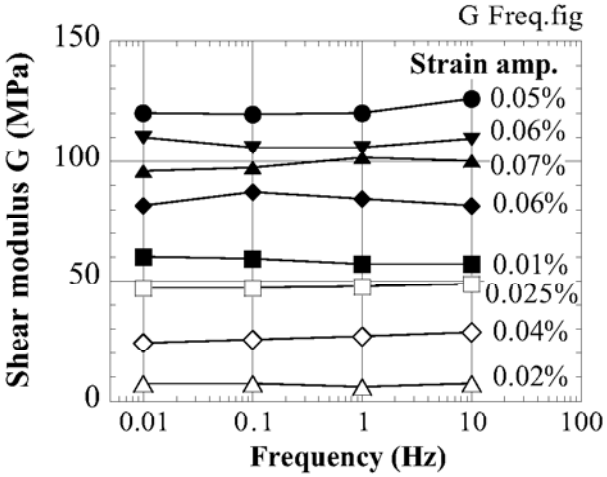

Fig. 10.23 Effects of loading frequency on modulus of clays (after Hara, 1973)

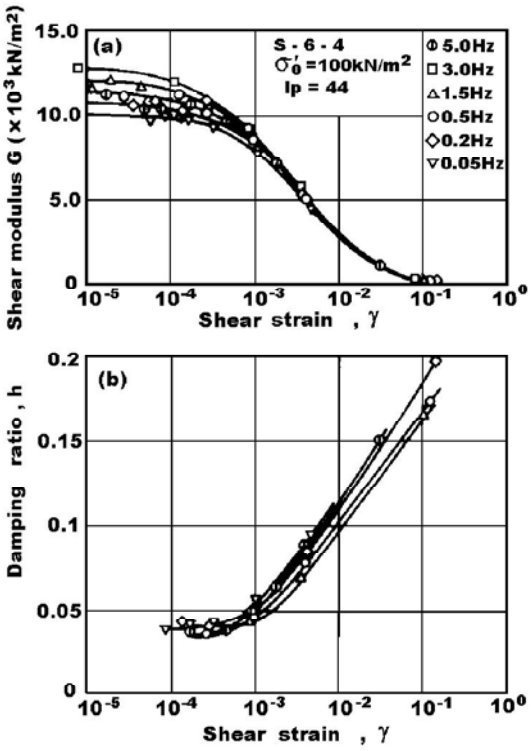

Fig. 10.24 Effects of loading frequency on dynamic properties of clays (Kokusho, 1982)

Thus, there are some effects of loading frequency on the cyclic stress–strain behavior of clays. However, these rate effects are not seriously taken in practice because other factors are more influential. Ellis et al. (2000) conducted resonant column tests to examine the effects of viscosity of pore fluid on damping ratio. Damping ratio increases by a few percent when viscosity increased by tens of times.

10.10 Effects of Plasticity on Cyclic Behavior of Clay

Clay has a thixotropic nature. Its shear rigidity and strength increase with time, because the cementation and bonding develop with time between particles. It is reasonable, therefore, that clays with a greater plasticity index (I_p) is more thixotropic than less plastic materials. Further, the bonding may be destroyed by cyclic loading with a relatively large strain amplitude. Hence, clay becomes softer with the number of cycles. This phenomenon is called "*degradation,*" which is important in behavior of offshore structures resting on clayey seabed during storms. The development of bonding is more substantial when clay is overconsolidated. An empirical formula is available for G_{max} of clay:

$$G_{max} = 625 \frac{OCR^k}{0.3 + 0.7e^2} \sqrt{P_a P'}, \quad (10.2)$$

in which P' stands for the effective mean principal stress of $(\sigma'_1 + \sigma'_2 + \sigma'_3)/3$, P_a is the atmospheric pressure (大気圧 ≈98 kPa) and OCR designates the overconsolidation ratio (Sect. 1.4). This formula works with any unit system. For the value of parameter k, see Fig. 10.25.

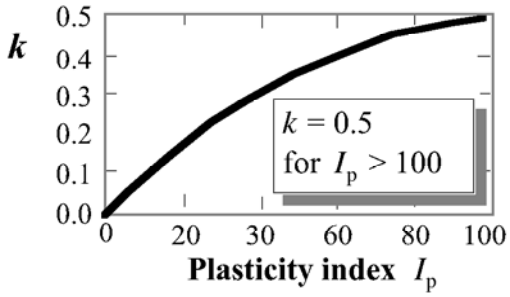

Fig. 10.25 Effects of OCR on G_{max} of clay (Hardin, 1978)

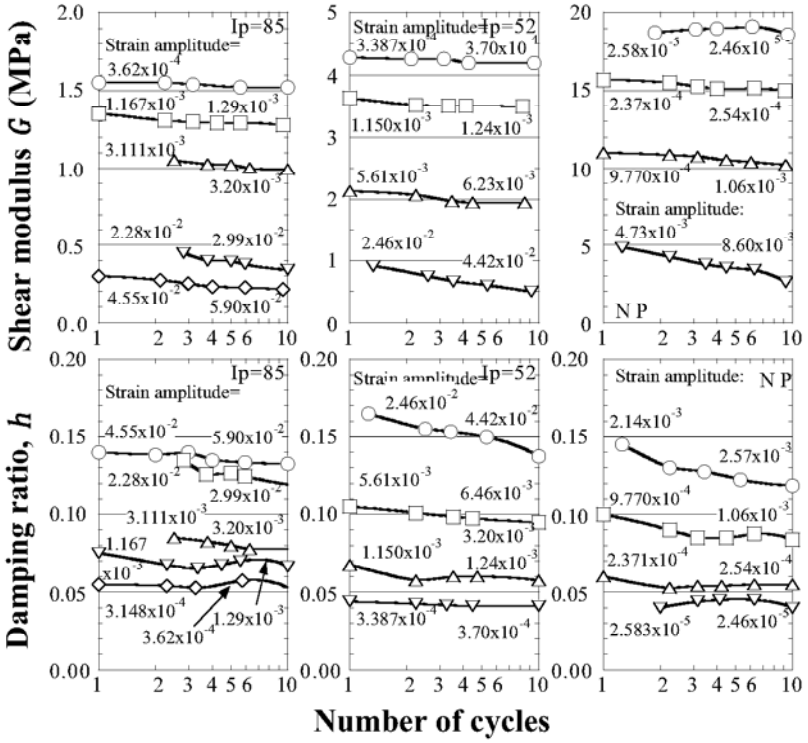

Fig. 10.26 Effects of plasticity on cyclic behavior of clay (Kokusho, 1982)

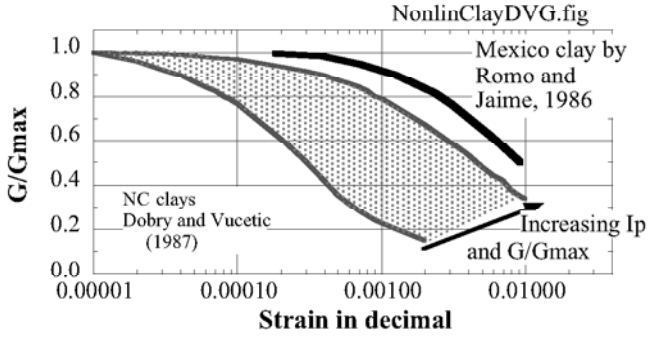

Fig. 10.27 Effects of I_p on G/G_{max} of clay (Dobry and Vucetic, 1987)

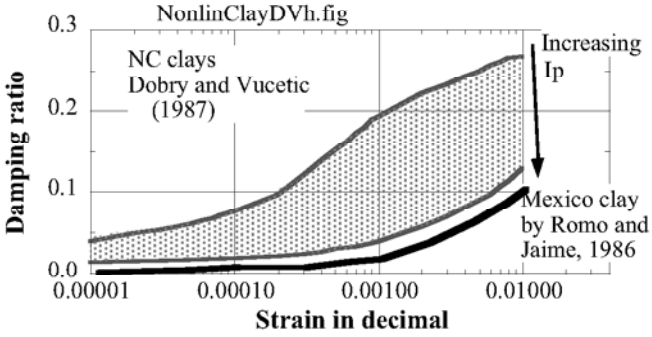

Fig. 10.28 Effects of I_p on damping ratio of clay (Dobry and Vucetic, 1987)

Kokusho (1982) studied that G and h (damping ratio) of Teganuma (手賀沼) clay decrease with the number of cycles (Fig. 10.26). It is more interesting in Fig. 10.26 that the specimens with greater I_p have smaller G and h; the smaller h suggests more elastic behavior. Dobry and Vucetic (1987) summarized this data and others to obtain Fig. 10.27 and Fig. 10.28, which indicate that the greater I_p is associated with less reduction of G/G_{max} and smaller damping ratio. The greater I_p is thus associated with more linear elastic behavior, suggesting less discrete nature of soil (Sect. 10.2). Note that I_p = 150–250 for Mexico City Clay, while I_p = 20–100 for other clays.

Hardin and Black (1968) studied the variation of G of NC (normally consolidated) clay with void ratio. Figure 10.29 indicates that G_{max} varies in proportion to $(2.973–e)^2/(1+e)$ and the square root of the isotropic consolidation pressure, $\sqrt{\sigma_0'}$. Note, however, that the parameter of 2.973 varies with type of clay. Figure 10.30 and Fig. 10.31 compare the variation of G_{max} of overconsolidated (OC) kaolinite (LL = 65.9% and I_p = 35%) and calcium-bentonite (LL = 120% and I_p = 60%). See that e–log P behavior of kaolinite is more elastic than that of bentonite during unloading and reloading. This difference seems consistent with the recoverable change of G_{max} of OC kaolinite.

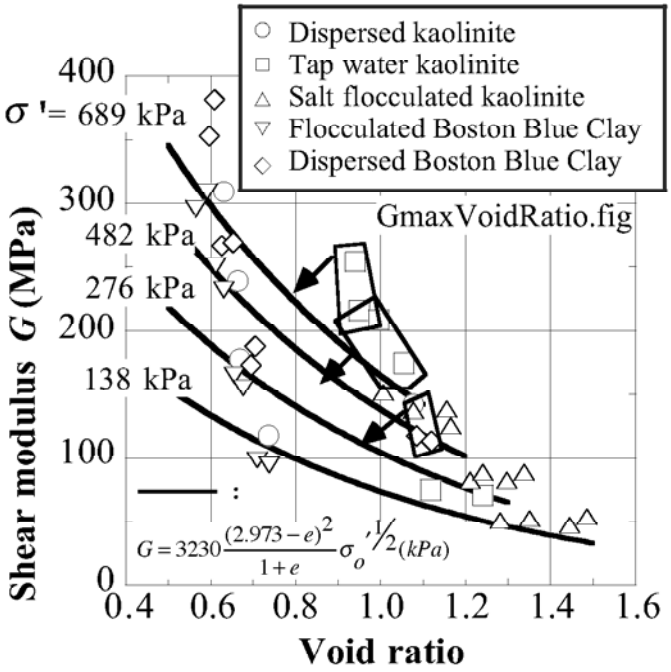

Fig. 10.29 Variation of G_{max} of clay with void ratio

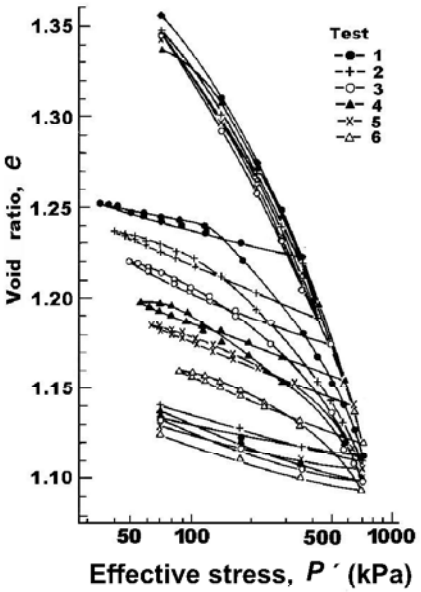

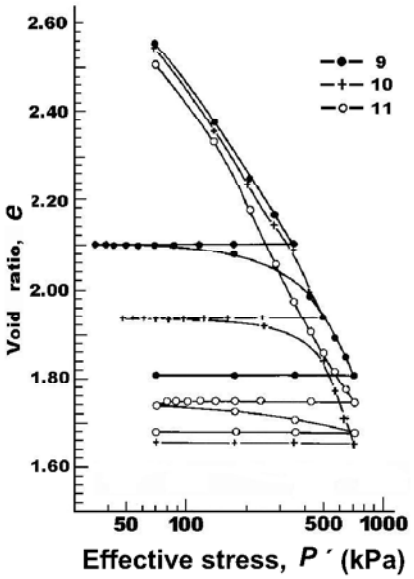

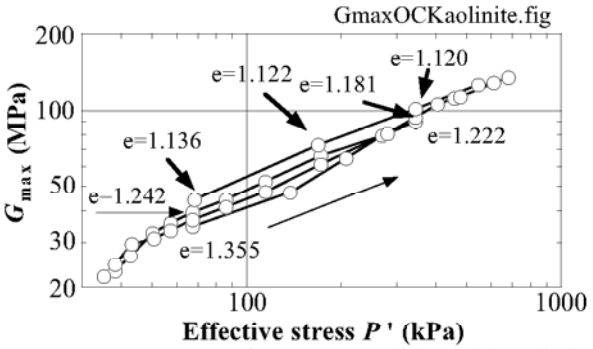

Fig. 10.30 G_{max} of overconsolidated kaolinite (Humphries and Wahls, 1968)

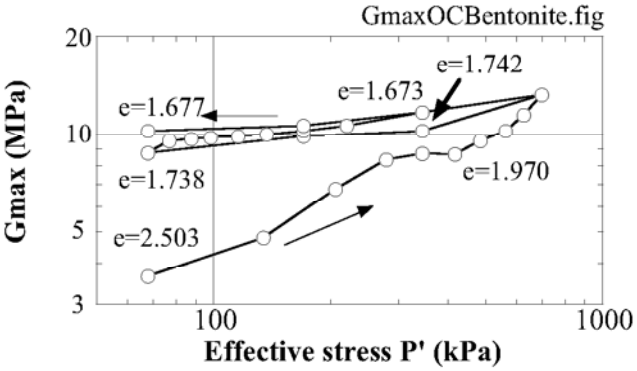

Fig. 10.31 G_{max} of overconsolidated bentonite (after Humphries and Wahls, 1968)

Bonding between clay particles develops gradually with time. This seems to increase G_{max} of clay with time as well. Afifi and Richart (1973) studied this time effect by running resonant column tests. Figure 10.32 indicates the stress history in which loading and unloading/reloading were carried out. The primary consolidation ceased at about 100 min. Figure 10.33 illustrates the time increase of G_{max} of NC samples. Although the primary consolidation was completed at 100 min, G_{max} kept increasing after 100 min without further densification. This suggests the effects of particle bonding together with possible minor rearrangement of particles, which can be called ageing.

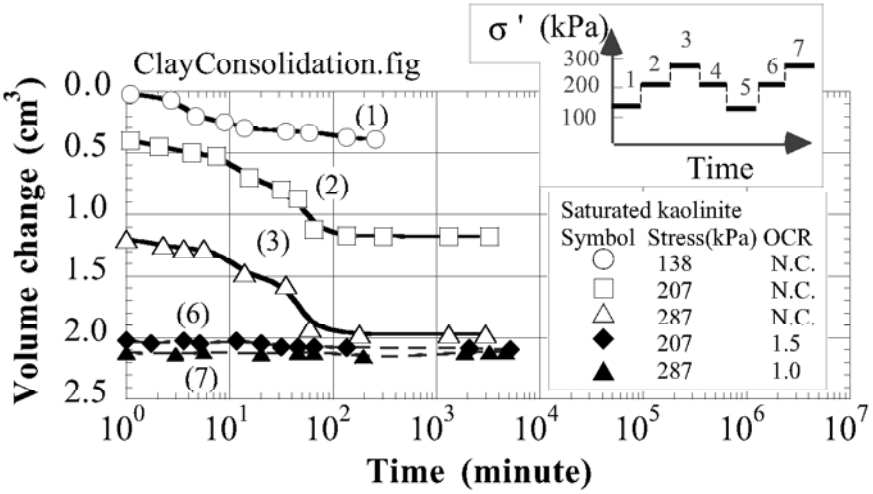

Fig. 10.32 Consolidation data of tested clay (Afifi and Richart, 1973)

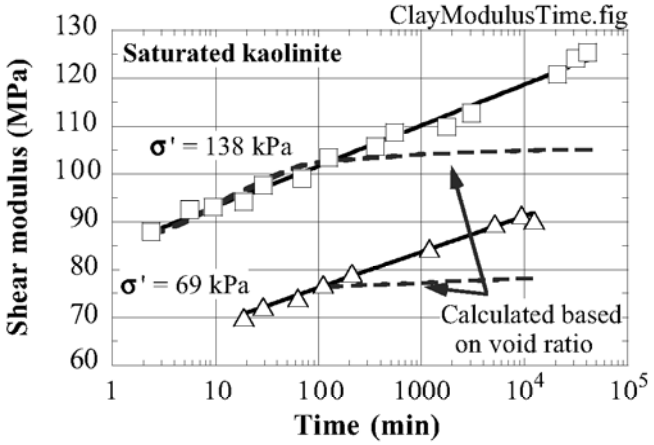

Fig. 10.33 Increase of G_{max} of clay with time (drawn after Afifi and Richart, 1973)

Kokusho (1982) compared $\Delta G/G_{1000}$ in his own tests with those by Afifi and Richart (1973) and Anderson and Woods (1976); Fig. 10.34. G_{1000} stands for G_{max} at 1,000 min and ΔG is the increase of G_{max} per one logarithmic cycle of time (e.g. from 1,000 to 10,000 min). The finer soils (smaller D_{50}; Fig. 1.3) show greater rate of increase in G_{max} probably due to ageing of clay contents. Finally , a good correlation was demonstrated between $\Delta G/G_{1000}$ and plasticity index (I_p); Fig. 10.35.

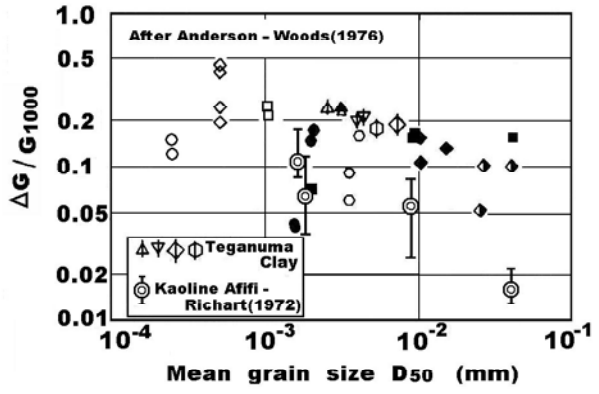

Fig. 10.34 Increase rate of G_{max} (Kokusho, 1982)

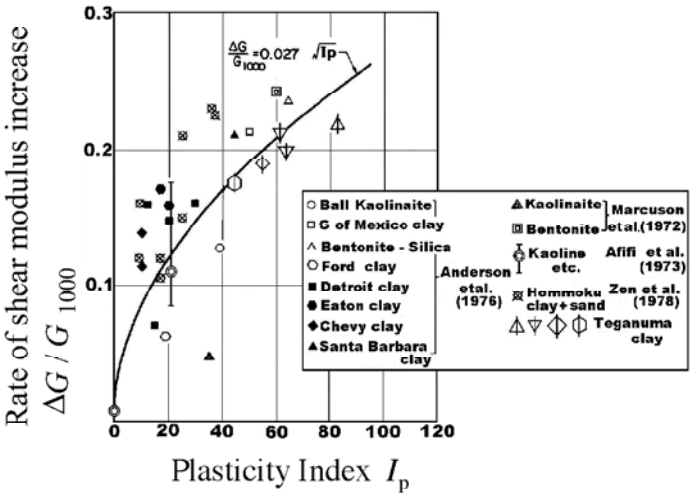

Fig. 10.35 Rate of increase in G_{max} changing with plasticity index (Kokusho, 1982)

The use of D_{50} in study of clay and silt has caused a problem in which true clay and silt with cohesion were confused with such a cohesionless fine material as mine tailing materials (Sect. 20.5). Information about clay and silt were often applied to tailings because the latter had a small value of D_{50} as well. Study in terms of plasticity index can solve this problem because the tailing material is non plastic.

10.13 Effects of Strain Amplitude on Shear Modulus of Clay

Since the modulus of clay decreases with the number of cycles (degradation; Sect. 10.14), G at a specified number of cycles has been studied by many people. The employed number is 10–20 depending upon researchers.

Figure 10.36 indicates the variation of G with the single amplitude of strain. The nonlinearity in clay is less significant than that in coarser materials. Figure 10.37 shows that the effects of I_p (plasticity index; Sect. 1.1) and OCR (overconsolidation ratio) on G/G_{max} vs. γ curve is not very important, although smaller OCR appears to be associated with more nonlinearity. A more detailed study in Fig. 10.38, however, suggests that a fixed G/G_{max} occurs at a larger strain amplitude when I_p increases; greater I_p reduces nonlinearity of clay. Finally, Fig. 10.39 shows that G/G_{max} is independent of the effective stress level.

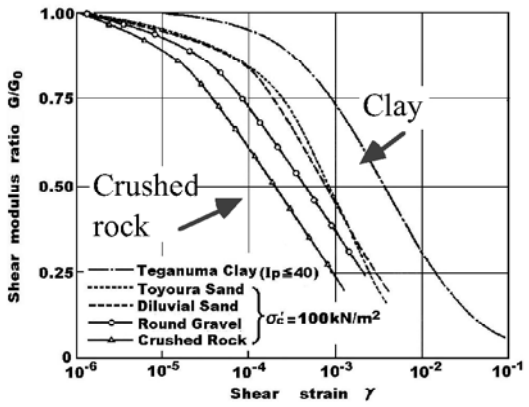

Fig. 10.36 Variation of G with strain amplitude (Kokusho, 1982)

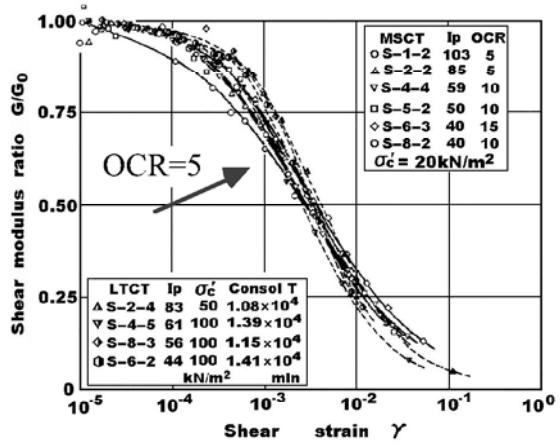

Fig. 10.37 Effects of I_p and OCR on G of clay (Kokusho et al. 1982)

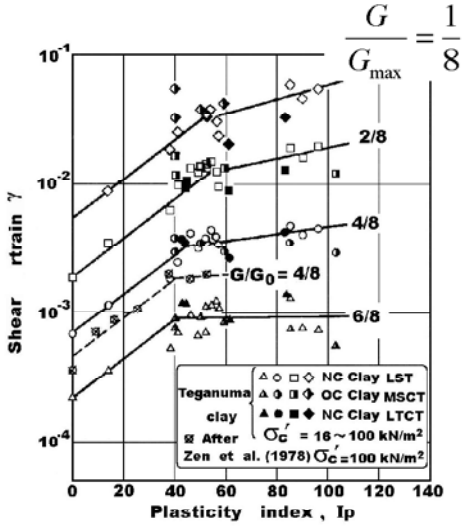

Fig. 10.38 Effects of I_p on nonlinearity of clay (Kokusho, 1982)

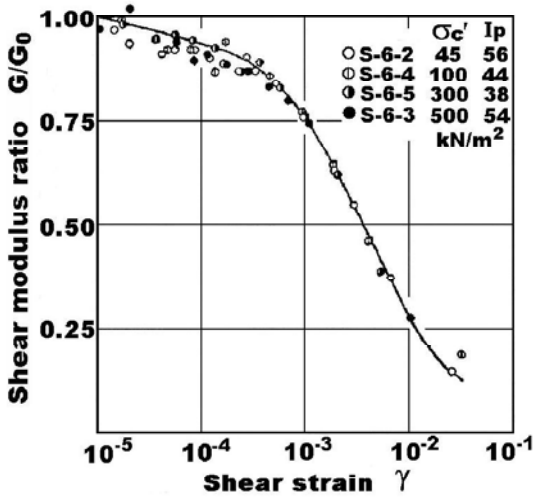

Fig. 10.39 Effects of confining pressure on G of clay (Kokusho et al. 1982)

10.14 Degradation of Shear Modulus of Clay

Degradation is a phenomenon in which shear modulus (rigidity) of clay decreases with the number of loading cycles (Dobry and Vucetic, 1987). An example of degradation is illustrated in Fig. 10.40 (see Fig. 10.8 as well). The decrease of shear modulus is important in the stability of foundation of offshore structures that are subjected to thousands of cycles of wave loads during heavy storms. Degradation is caused probably by (1) the accumulation of excess pore water pressure and decrease of effective stress, and (2) breakage of bonding between clay particles. Osipov et al. (2005) took an electron-microscopic photograph of a clay bridge connecting sand grains. Practical engineers may consider degradation in such a manner as

$$\delta \equiv \frac{G(\text{Nth cycle})}{G(\text{1st cycle})} = N^{-t}, \qquad (10.3)$$

in which N is the number of cycles while t is called the degradation parameter.

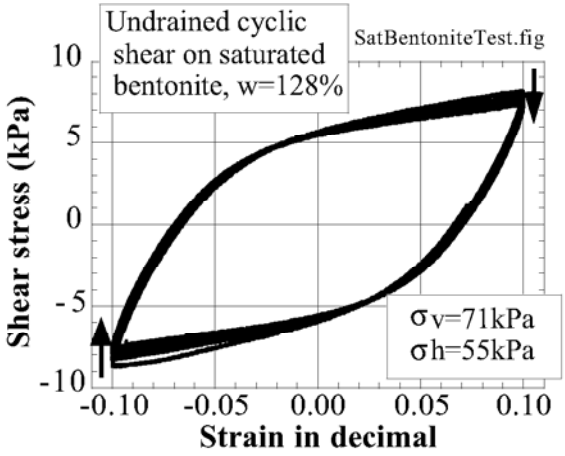

Fig. 10.40 Example of degradation in undrained cyclic shear of bentonite clay

Dobry and Vucetic (1987) reported values of δ at a variety of OCR (overconsolidation ratio) and strain amplitude. Figure 10.41 indicates that the shear modulus is possible to decrease to 70 or 80% of the initial value when a substantial amplitude of strain is repeated 100 times or more. The greater values of t suggests that the pore pressure increase and the breakage of bonding are substantial when the strain amplitude is large in young clay with smaller values of OCR (Fig. 10.42).

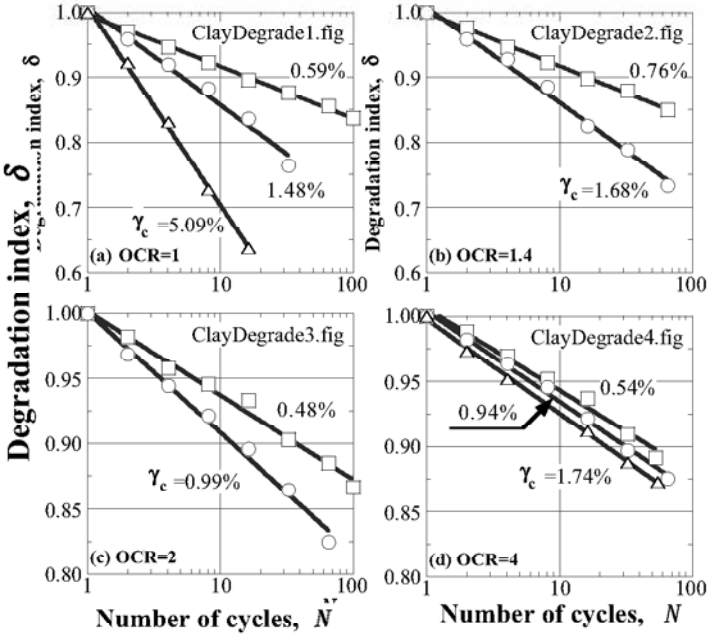

Fig. 10.41 Observed degradation (Dobry and Vucetic, 1987)

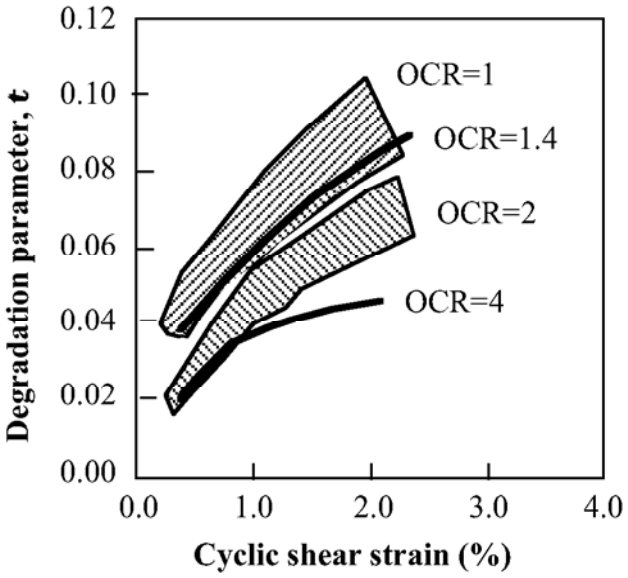

Fig.10.42 Variation of degradation parameter with OCR and strain amplitude (drawn after Dobry and Vucetic, 1987)

10.15 Damping Ratio of Clay

Damping ratio seems to be less affected by many factors than shear modulus. A limited rate-dependency was indicated in Sect. 10.9. The type of soil, however, appears relatively important as Fig. 10.43 reveals that the damping ratio of clay is smaller than that of coarser materials. This is probably because clay is more continuous than sand and gravel.

Figure 10.44 by Kokusho et al. (1982) indicates test results on undisturbed clay specimens that the damping ratio is not significantly affected by the effective stress level. What is peculiar in this figure is that the higher effective stress caused slightly larger damping ratio, opposite from what was found for sand (Fig. 10.21). Although not clearly known, one of the possible reasons for this may be that the greater amount of consolidation volume change under the higher stress destroyed the interparticle bonding of clay.

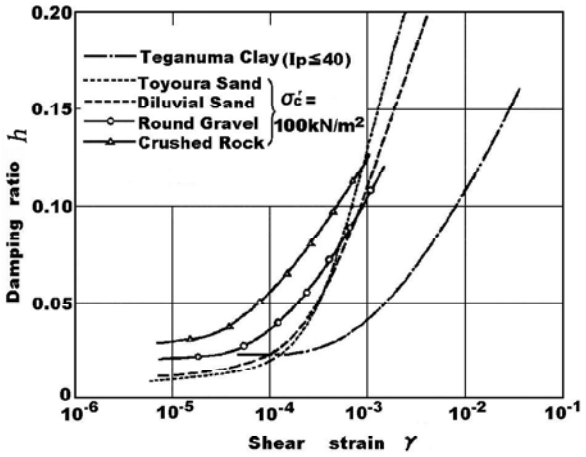

Fig. 10.43 Damping ratio of clay, sand, and gravel (Kokusho, 1982)

Figure 10.45 demonstrates that NC and OC clays are of more or less similar magnitude of damping ratio.

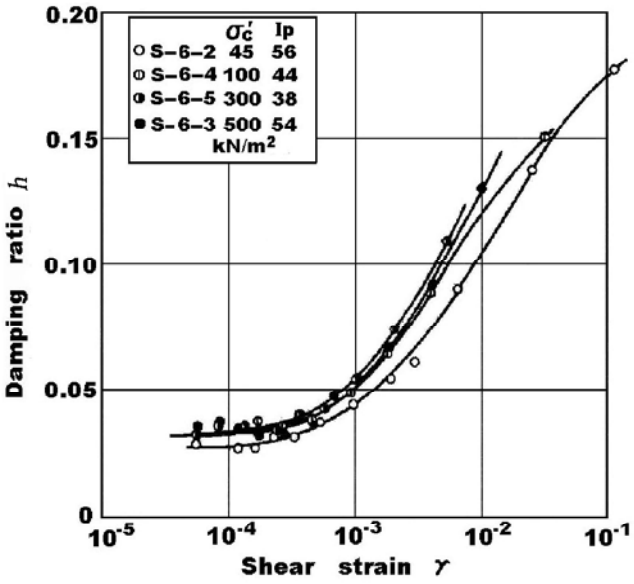

Fig. 10.44 Effects of confining pressure on damping ratio of clay (Kokusho, Yoshida and Esashi, 1982)

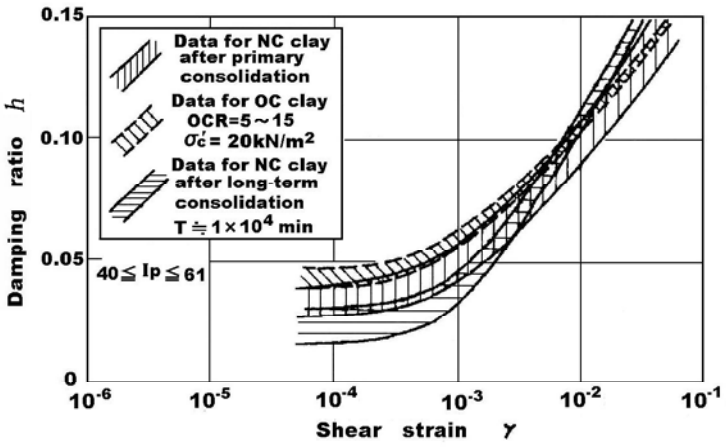

Fig. 10.45 Damping ratio of NC (Normally Consolidated) and OC (Overconsolidated) clays (Kokusho et al. 1982)

10.16 Effects of Consolidation Time on Damping of Clay

Marcuson and Wahls (1978) studied the damping ratio at a small strain range (γ=0.0012–0.0048%). Both drained and undrained tests were run on kaolinite specimens as well as more plastic bentonite samples. It was shown by all tests in Figs. 10.46–10.49 that the damping ratio decreases as the consolidation time becomes longer. This may suggests that particle bonding is built as time passes and that clay becomes a more continuous material. In the figures, the T ratio is defined by

$$T \text{ ratio} = \frac{\text{Consolidation time}}{\text{Time for 100\% primary consolidation}}.$$

Note further that damping ratio is greater under lower effective stress.

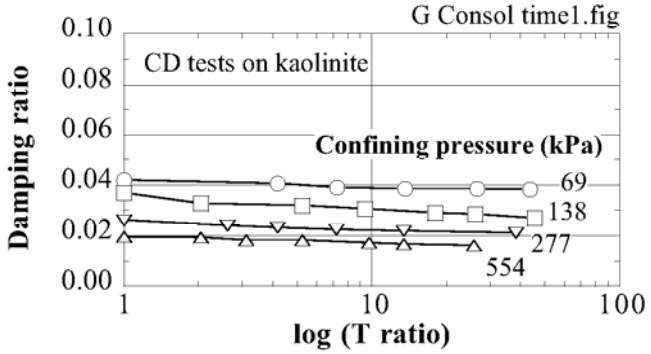

Fig. 10.46 Change in damping ratio of kaolin with time in drained tests (Marcuson and Wahls, 1978)

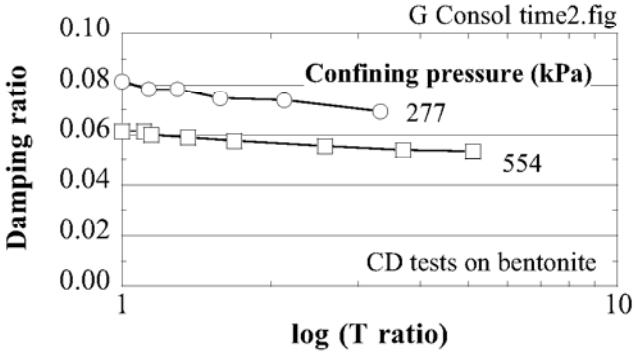

Fig. 10.47 Change in damping ratio of bentonite with time in drained tests (Marcuson and Wahls, 1978)

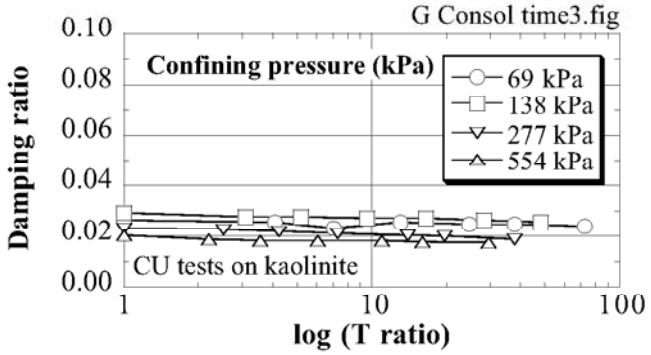

Fig. 10.48 Change in damping ratio of kaolin with time in undrained tests (Marcuson and Wahls, 1978)

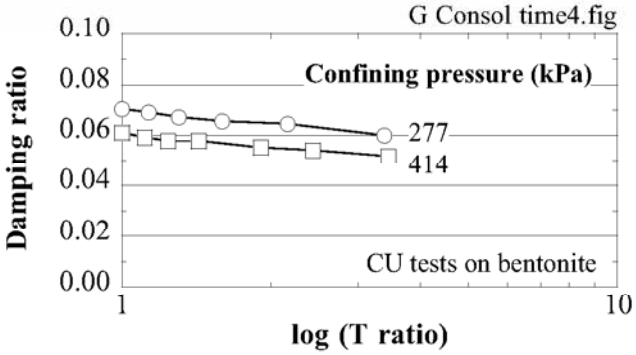

Fig. 10.49 Change in damping ratio of bentonite with time in undrained tests (Marcuson and Wahls, 1978)

10.17 $G-\gamma$ and $h-\gamma$ Curves of Undisturbed Samples

Many data on nonlinear dynamic deformation characteristics of soils were obtained from drained tests on laboratory-reconstituted specimens. Since the effects of age and drainage are not negligible in real ground, however, nonlinearity data obtained from more realistic test conditions have been desired. In this regard, Yasuda and Yamaguchi (1985) summarized those data obtained from undrained tests on undisturbed samples and proposed an empirical rule:

$$\frac{G}{G_{\max}} = \left(A_1 + A_2 \log_{10} D_{50}\right) \times P'^{\left(B_1 + B_2 \log_{10} D_{50}\right)} \quad \text{and} \quad h = \left(C_1 + C_2 \log_{10} D_{50}\right) \times P'^{\left(D_1 + D_2 \log_{10} D_{50}\right)},$$

where D_{50} is the mean particle size of sand (mm) and P' the effective mean principal stress (kgf/cm^2);

$$P' = \left(\sigma'_1 + \sigma'_2 + \sigma'_3\right)/3 = \left(1 + 2K_0\right)\sigma'_{vertical}/3 \quad \text{for in-situ } K_0 \text{ consolidation.}$$

The parameters of A_1 to D_2 were determined empirically as shown in Table 10.1. Consequently,

Table 10.1 Parameters in Yasuda–Yamaguchi empirical formulae

Shear strain γ_a	A_1	A_2	B_1	B_2	C_1	C_2	D_1	D_2
10^{-4}	0.827	–0.044	0.056	0.026	0.035	0.005	–0.0559	–0.258
3×10^{-4}	0.670	–0.068	0.184	0.086				
10^{-3}	0.387	–0.099	0.277	0.130	0.136	0.036	–0.375	–0.173
3×10^{-3}	0.189	–0.089	0.315	0.147				
10^{-2}	0.061	–0.054	0.365	0.167	0.234	0.037	0.000	0.000
3×10^{-2}	0.041	–0.019	0.403	0.183				

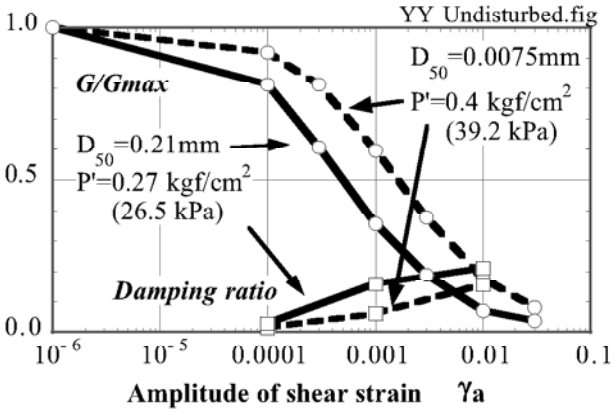

Fig. 10.50 Example of predicted characteristics of undisturbed samples

- $G_{\max}$ in their study is the shear modulus at a strain amplitude of 10^{-6} (=0.0001%).
- B_1=B_2=D_1=D_2=0 when $D_{50} < 0.007$ mm.
- The original database for this study was obtained for a limited condition of $0.2 \le P' \le 3$ kgf/cm^2 $\left(19.6 \le P' \le 294\ kPa\right)$ and $0.002 \le D_{50} \le 1.0$ mm.
- Predicted G and damping ratio are indicated in Fig. 10.50. Both sandy and clayey materials were studied.
- When D_{50} is unknown in practice, its rough estimate may be given below:
  0.4 mm for coarse gravelly sand, 0.3 mm for medium sand, 0.2 mm for fine sand, 0.1 mm for silty sand, 0.04 mm for sandy silt, 0.03 mm for clayey sand, 0.007 mm for silt, and 0.005 mm for clayey silt.
- All the ideas given in this section may include significant error due to their approximate nature.
- B_1+$B_2 \log_{10}(D_{50})$ is positive, indicating that $G/G_{\max}$ is greater when P' increases.
- Similarly, D_1+$D_2 \log_{10}(D_{50})$ is negative, suggesting that the damping ratio decreases as P' increases.
- Examine that $G/G_{\max}$ decreases and damping ratio increases for coarser materials (greater D_{50}).

Although gravelly subsoils are highly stable and their shear strength is hardly discussed, the seismic behavior of nuclear power plant facilities has been a problem. While buildings of power plants to date are situated on a base rock, such important facilities as intake channels of emergency cooling water may be placed on a relatively softer layer. A gravelly layer is preferred to less stable sand and clay.

The safety of a nuclear power plant is absolutely important. Therefore, a seismic response analysis of important facilities has been conducted intensely by using an equivalent linear technique. Because of this reason, the dynamic deformation characteristics of gravelly soils have been studied in detail. Another important application of this study is the seismic behavior of rock-fill dams (Fig. 10.51).

- Kokusho (1982) carried out a series of cyclic shear tests on gravelly materials by using a large triaxial device that measured 30 cm in sample diameter.
- Figure 10.52 reveals test results on crushed rock (砕石) with D_{50} about 30 mm. G_{max} varies with $(2.17-e)^2/(1+e)$ and $\sigma_c'^{0.55}$; σ_c' being the isotropic consolidation pressure.
- Figures 10.53 and 10.54 compare the crushed rock with finer Toyoura sand (D_{50} being about 0.18 mm). See that the coarser material has smaller G/G_{max} and greater damping ratio, which imply more nonlinearity.
- Since a gravelly layer is normally dense, the effects of excess pore water pressure is neglected.

Fig. 10.51 Construction of rock fill dam

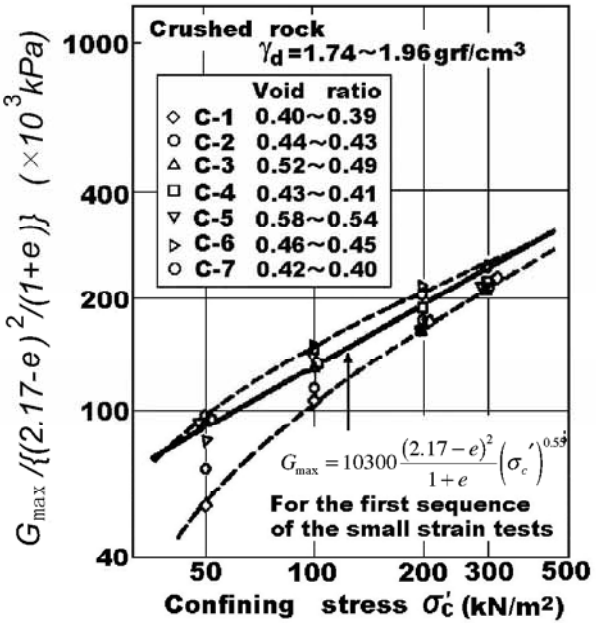

Fig. 10.52 Variation of G_{max} at small strain with void ratio and effective confining pressure (Kokusho, 1982)

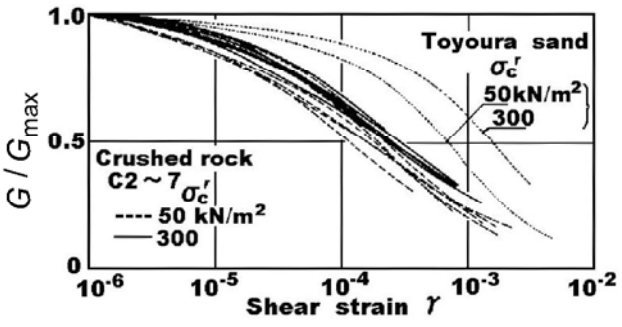

Fig. 10.53 G/G_{max} of crushed rock (Kokusho, 1982)

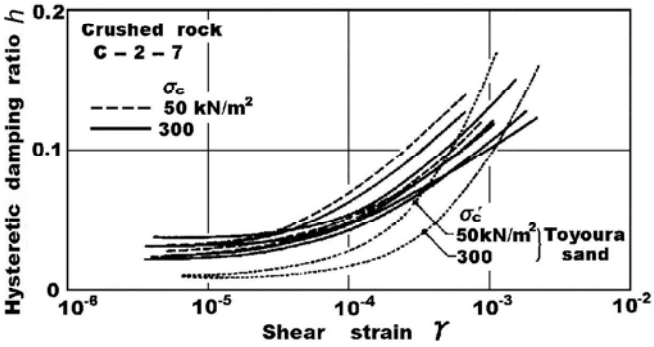

Fig. 10.54 Damping ratio of crushed rock (Kokusho, 1982)

The nonlinear stress–strain behavior is measured precisely by running triaxial or other shear tests on undisturbed specimens that are collected in situ. The quality of collected samples is affected by stress history that occurs in samples. Although it is desirable that the stress-state in the field is kept unchanged during sampling, transportation to laboratory, and preparation of testing, it is impossible in practice. Among major sources of sample disturbance are the change of stress state from the anisotropic one in the ground to the isotropic one at the surface (Fig. 10.55) and the undesired force generated by penetration of a sampling machine into soil. Change of stress as illustrated in Fig. 10.55 is inevitable.

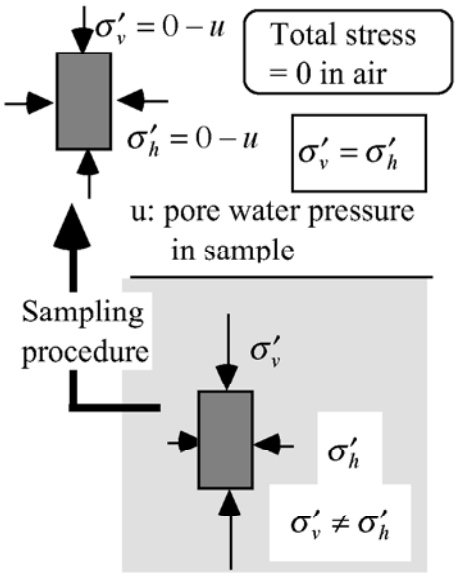

Fig. 10.55 Change of underground effective stress state to subaerial state

Figure 10.56 illustrates the mechanism of a soil sampler. At the bottom of a bore hole, the piston is fixed to a facility at the ground surface, and the sampling tube is pushed into soil.

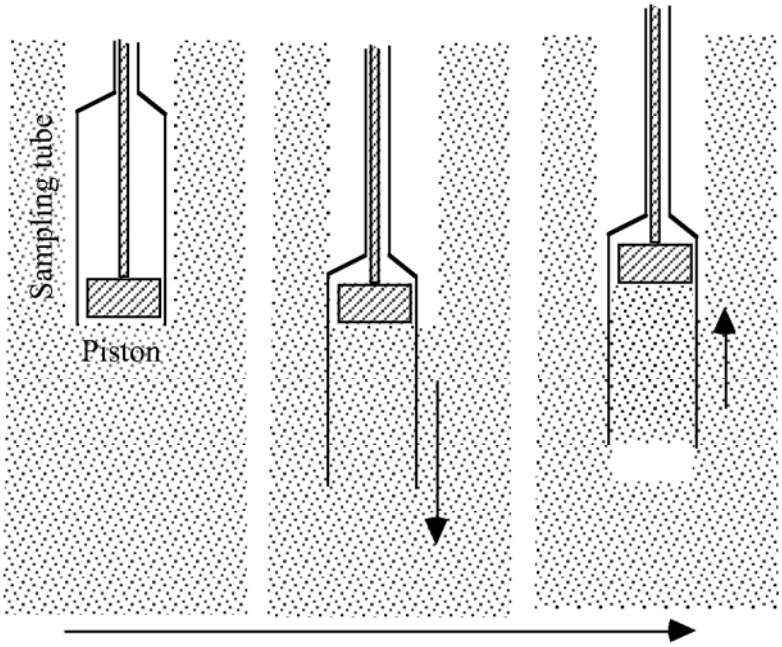

Fig. 10.56 Mechanism of soil sampling at bottom of bore hole

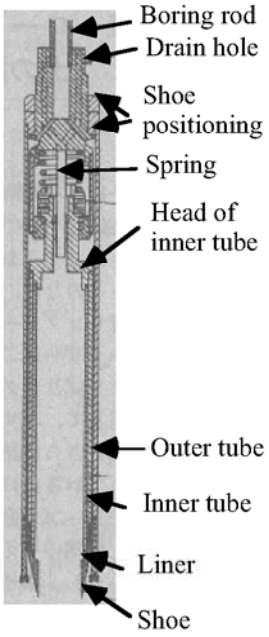

Fig. 10.57 Triple-tube sampler for sand (Japanese Geotechnical Society, 1995)

Efforts have been made to reduce the effects of penetration of a sampling tube into ground. In a triple-tube sampler for loose sandy soils (Fig. 10.57), the outer tube removes unnecessary soil in order to make easy the penetration of the inner tube: less force and less disturbance. The inner tube has a liner inside (third tube made of vinyl chloride or acryl), which contains a collected sample.This device is, however, not able to collect samples of extremely loose sand (SPT-N < 2, for example). Sand falls down from the tube. It seems necessary to hold sand by closing the bottom of the tube. FIgure 10.58 shows extrusion of an undisturbed soil sample from a tube (Fig. 10.58).

Collecting blocks of specimen is a cheap method of sampling if it is possible to approach the target soil layer at the bottom of an excavation work (Fig. 10.59). Collected sandy samples are frozen in an insulated container by using dry ice and are transported without additional disturbance. Make sure that unfrozen pore water is drained out of a specimen because freezing increases the volume of water. Otherwise, ice pushes sand grains, disturbs the granular structure, and makes sand softer. Fig. 10.60 shows a block sampling of a large size. The collected specimen was later used for centrifugal model tests (Sect. 24.11).

Clay sample (SPT-$N > 4$) is often collected by a thin wall sampler (Fig. 10.61). This device has a very thin (approx. 2 mm) sampling tube, which minimizes the soil particle movement during penetration. A tightly fixed piston is important to avoid sample disturbance.

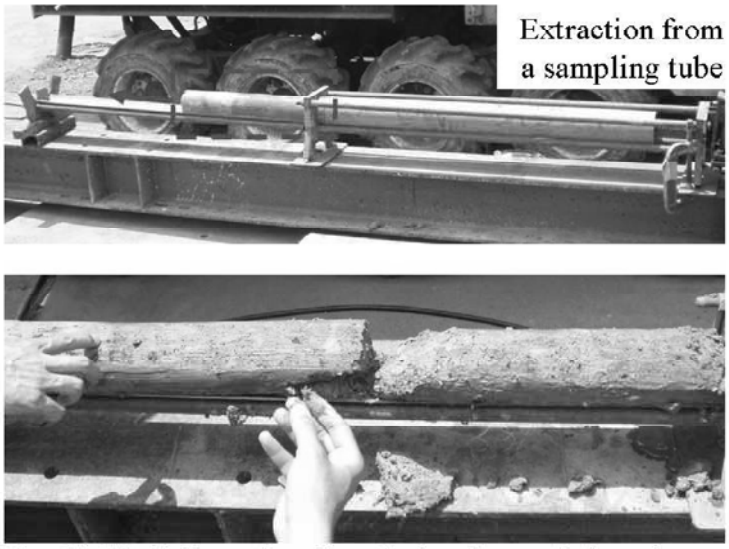

Fig. 10.58 Collected undisturbed soil sample by tube sampling method

Fig. 10.60 Large block sampling of Yurakucho sand in Tokyo by Fujiwara et al. (2005)

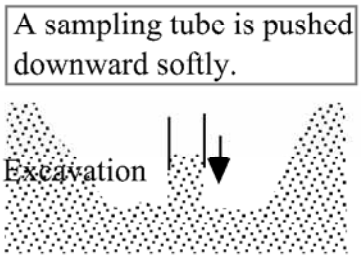

Fig. 10.59 Block sampling

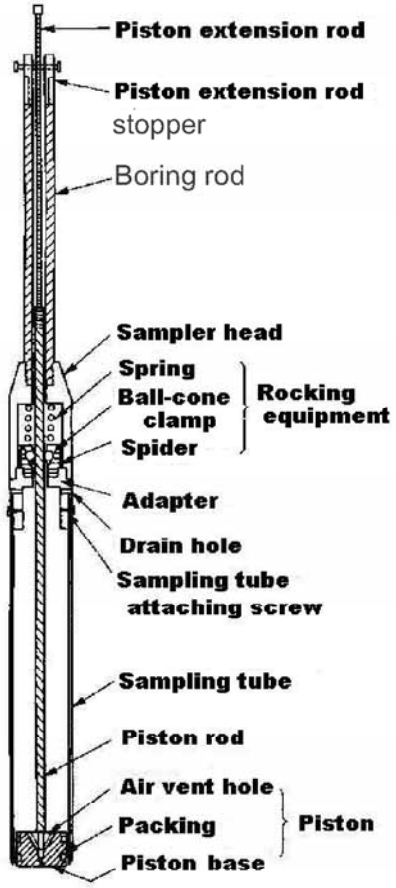

Fig. 10.61 Thin-wall sampler for clay with fixed piston (Japanese Geotechnical Society, 1995)

A recent development in undisturbed sampling is found in freezing technique. For its details, refer to Sect. 10.20. Another achievement is the use of polymer liquid during cutting soil core (Tani and Kaneko, 2006). This liquid solidifies around a sample and produces a confining effect so that disturbance is minimized. This method was successfully applied to sampling of alluvial gravelly sand with SPT = 15–30 with a large size of 160 mm in diameter and 1,600 mm in length.

For the quality of undisturbed samples, refer to Sect. 10.21.

10.20 Freezing Technique of Sand Sampling

A better sample quality of loose sand is achieved by the technique of in-situ freezing (Yoshimi et al. 1985, 1994, 1996); Fig. 10.62. This technique is, therefore, employed for investigation of liquefaction hazard. The frozen pore water (ice) prevents any mechanical disturbance in granular structure (粒子構造) of sand. Care should be taken to start freezing from one end of soil mass and pushing the freezing front to proceed to the other end. Thus, unfrozen water is drained out. Otherwise, volume increase of ice pushes sand particles outwards and changes the granular structure, leading to disturbance in mechanical nature of sand. For the same reason, freezing of impervious clayey ground is not advisable.

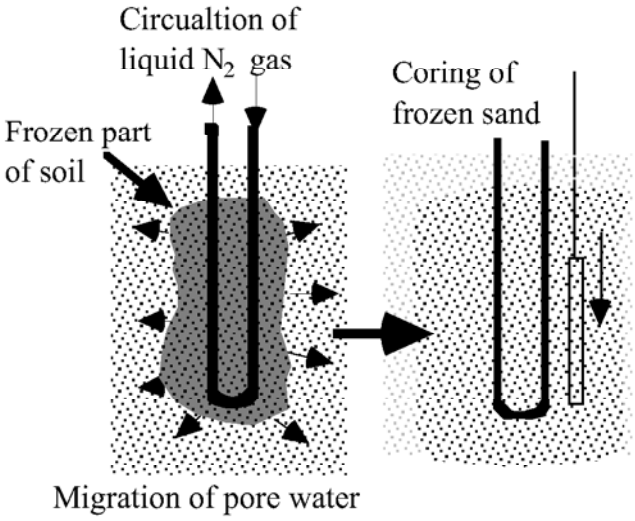

Fig. 10.62 In-situ freezing of sandy ground

The practice of freezing of gravelly sandy ground and the appearance of collected sample are demonstrated in Fig. 10.63 and Fig. 10.64. See the section of a large grain that was cut smoothly by a diamond bit of a coring device. This ideal technique of sand sampling is more expensive than thin-wall sampling, and, therefore, is employed in relatively important projects.

Freezing technique is frequently used for investigation of liquefaction potential in important projects.

It seems that less attention has been paid to the thawing process of a frozen specimen. Free flow and sufficient supply of pore water are needed in thawing parts of a specimen. Otherwise, an open space with air may be formed in a specimen or the specimen volume may contract due to volume contraction during melting of ice to water.

Fig. 10.63 Practice of in-situ freezing (in Uozaki)

Fig. 10.64 Gravel particles at the surface of collected frozen specimen

10.21 Extent of Sample Disturbance

It is important to assess the extent of sample disturbance caused by the present state of "undisturbed sand sampling." At present, comparison of G_{max} at small strain obtained from laboratory tests on "undisturbed" specimen and the in-situ G/G_{max} obtained from V_s (down-hole or suspension survey) meets this requirement. Figure 10.65 compares $G_{max,L}$ from laboratory tests on undisturbed specimens and $G_{max,F}$ from in-situ measurement of S-wave velocity ($V_s = \sqrt{G_{max}/\rho}$). Unfortunately, they are not necessarily equal to each other.

Symbols of ○ and □ in Fig. 10.65 compares values of laboratory G_{max} values and those determined from S-wave velocity. The former was obtained from laboratory tests on samples collected by so-called "undrained" tube sampling (Sect. 10.19) and is possibly subject to sample disturbance, while the latter is free of such an error. It is illustrated therein that laboratory G_{max} ($G_{max,L}$) is greater than field G_{max} ($G_{max,F}$) when they are relatively small. This is probably because the concerned soil was loose and is subject to densification caused by sample disturbance. G_{max} of densified soil ($G_{max,L}$) is greater than the original $G_{max,F}$. Conversely, dense insitu soil is subjected to loosening induced by disturbance. Therefore, the relatively greater G_{max} of in-situ soil is reduced after loosening. Thus, the quality of what is called undisturbed sampling is not yet fully reliable.

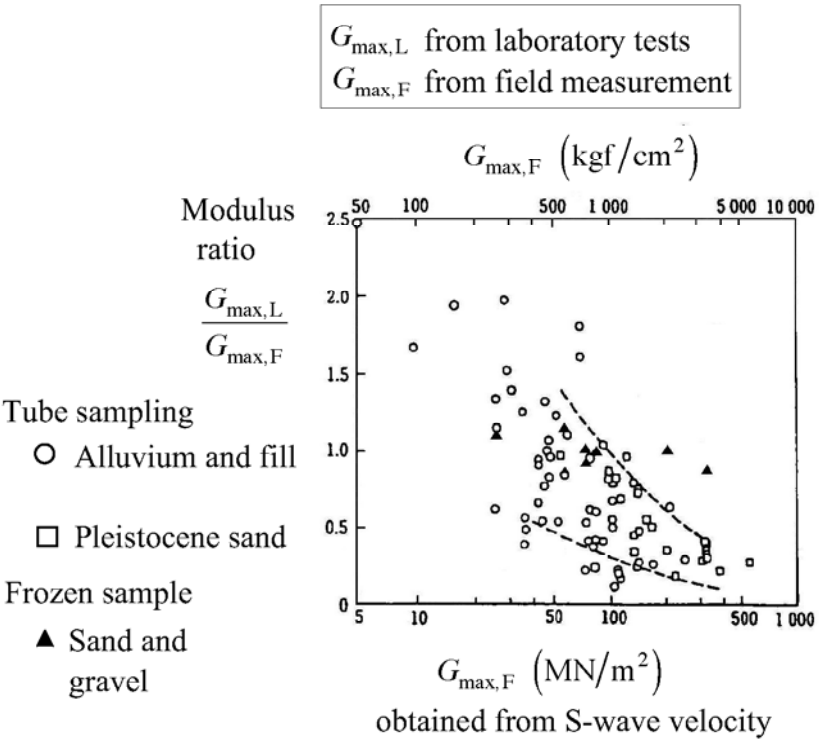

Fig. 10.65 Comparison of shear modulus at small strain obtained from laboratory tests on undisturbed samples and from in-situ downhole survey (Tokimatsu, 1995; data was added to the original figure by Yasuda and Yamaguchi, 1984)

It is advisable, therefore, to determine G_{max} from field investigation (direct measurement of V_s). On the other hand, the nonlinearity (change of G with strain amplitude and damping ratio) is assessed by laboratory testing of undisturbed samples because those data appears less sensitive to many factors as have been shown so far.

It is interesting in Fig. 10.65 that G_{max} of undisturbed samples collected by freezing technique (▲) is in good agreement with the field data ($G_{max,F}$). It appears that freezing technique of sampling can avoid efficiently the bad effects of sample disturbance.

Hatanaka et al. (1995) compared liquefaction resistance of frozen samples and that of conventional samples (triple tube sampler in Fig. 10.60). It was found that tube sampling generally densifies the collected sand and decreases its liquefaction resistance.

10.22 Correlation Between Surface Velocity and Strain in Subsoil

The propagation of S wave is governed by the following equation:

$$\frac{\partial^2 u}{\partial t^2} = V_s^2 \frac{\partial^2 u}{\partial z^2}, \tag{10.4}$$

in which u is the displacement and V_s is the wave propagation velocity. First when the wave propagates in one direction (positive direction of z coordinate), the solution of (10.4) is given by

$$u = F(t - z/V_s), \tag{10.5}$$

where F is an arbitrary function of $t - z/V_s$. Hence, velocity, v, and shear strain, γ, are given by

$$v = \frac{\partial F}{\partial t} = F'(t - z/V_s) \quad \text{and} \quad \gamma = \frac{\partial F}{\partial z} = -F'(t - z/V_s)/V_s = -v/V_s \tag{10.6}$$

where "F'" denotes derivative of F. Therefore, it is possible to assess the magnitude of strain by monitoring the velocity time history and somehow measuring independently the value of V_s (soil investigation).

In a horizontal soil deposit subjected to horizontal shaking, there are always two components (i.e., upward and downward propagations) of soil displacement as discussed in Sect. 4.1. Hence, the assessment of subsurface strain is not very simple. In the simplest case when harmonic shaking occurs,

$$u(t,z) = U_0 \cos\frac{\omega z}{V_s} e^{i\omega t} \text{ (Sect. 4.6)}, \quad v(t,z) = \frac{\partial u}{\partial t} = i\omega U_0 \cos\frac{\omega z}{V_s} e^{i\omega t}, \quad \text{and}$$
$$\gamma(t,z) = \frac{\omega}{V_s} U_0 \sin\frac{\omega z}{V_s} e^{i\omega t}. \tag{10.7}$$

Hence, the surface velocity amplitude and the subsurface strain amplitude maintain a simple proportionality.

$$\left|\frac{\gamma(t,z)}{v(t,z=0)}\right| = \frac{\tan\dfrac{\omega z}{V_s}}{V_s}. \tag{10.8}$$

Therefore, the greater velocity implies the larger strain in soil and probably the more significant damages in different facilities.

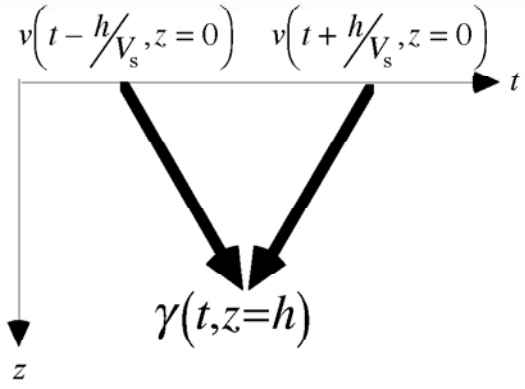

Fig. 10.66 Assessment of strain in subsoil by using surface velocity records (idea by Tokimatsu et al., 1989)

More generally, the solution of wave propagation is given by

$$u = E(t + z/V_s) + F(t - z/V_s)$$
$$v(t,z) = E'(t + z/V_s) + F'(t - z/V_s) \tag{10.9}$$
$$\gamma(t,z) = \{E'(t + z/V_s) - F'(t - z/V_s)\}/V_s.$$

Since the strain is zero at the free ground surface ($z = 0$),

$$E' = F'. \tag{10.10}$$

According to Tokimatsu et al. (1989), therefore, the strain at the depth of $z = h$ can be assessed by using the record of surface velocity as well as (10.10):

$$\begin{aligned}\gamma(t, z = h) &= \left\{E'\left(t + h/V_s\right) - F'\left(t - h/V_s\right)\right\}/V_s \\ &= \left\{E'\left(t + h/V_s\right) + F'\left(t + h/V_s\right) - E'\left(t - h/V_s\right) - F'\left(t - h/V_s\right)\right\}/\left(2V_s\right) \\ &= \left\{v\left(t + h/V_s, z = 0\right) - v\left(t - h/V_s, z = 0\right)\right\}/\left(2V_s\right). \end{aligned} \tag{10.11}$$

This idea was practiced by Tokimatsu et al. (1989) and is illustrated in Fig. 10.66. Moreover, V_s and, consequently, the shear modulus ($G = \rho V_s^2$) were determined separately by depicting the predominant period of surface motion records, T. Assuming that this T is equal to the natural period of the surface deposit, $V_s = 4h/T$ (Sect. 4.5 Exercise 1). Thus, it became possible to study G *vs. strain* relationship from the field observation. A good agreement in strain effects was obtained, consequently, between the field investigation and laboratory tests.

Bentonite clay is used widely as a buffer material in municipal waste landfill and probably in a repository of nuclear waste in future. Although its seismic behavior is important, there are few experimental information (see G_{max} data on Ca-bentonite in Fig. 10.31). In particular, much has not been known about the behavior of water-saturated Na–bentonite (sodium bentonite) that swells significantly upon water submergence. This is because of difficulties in experiments in which water saturated bentonite has to be produced from a slurry and consolidation time could be as long as 10 years for a laboratory specimen due to the low permeability and significant volume compression.

In literatures, Chijimatsu et al. (1999) produced water-saturated bentonite samples for permeability tests. The sample height in their study was, however, only 10 mm, which is not sufficient for triaxial tests. Noteworthy is the extremely patient studies by Mesri and Olson (1970) as well as Olson (1974) in which montmorillonite (bentonite) samples were consolidated from slurry. Consolidation time was longer than 1 year and triaxial tests lasted for more than 13 years.

Specimens of water-saturated Na bentonite was produced recently by Nakamura et al. (2007). They produced a new consolidation tank for highly compressible bentonite slurry in which drainage occurs in a radial direction of a hollow cylindrical specimen towards the drainage pipe at the center (Fig. 10.67). Since this drainage path is merely 5 cm in length and is much shorter than the 1-m maximum thickness of the bentonite slurry, the consolidation time is drastically reduced. The consolidation theory states that the time required for the completion of consolidation is proportional to the square of the size (1.14).

Figure 10.68 indicates the shape of a hollow cylindrical bentonite specimen after 3-month consolidation in the tank. This specimen was further trimmed to fit a torsion shear device (Sect. 18.8), consolidated again in the device for several days and tested under cyclic shear loading.

Figure 10.69 indicates the variation of G/G_{max} and damping ratio of water-saturated bentonite specimen. Since this study was related with nuclear waste problems, the original Na bentonite was mixed with 30% of silica sand. Hence, the plasticity index of the tested material was reduced to 251 %, which was lower than that of the original bentonite (more than 400 %). By comparing the values in this figure with data of other soils (Figs. 10.27 and 10.28), it is found that G/G_{max} of bentonite is greater than those of other soils, and

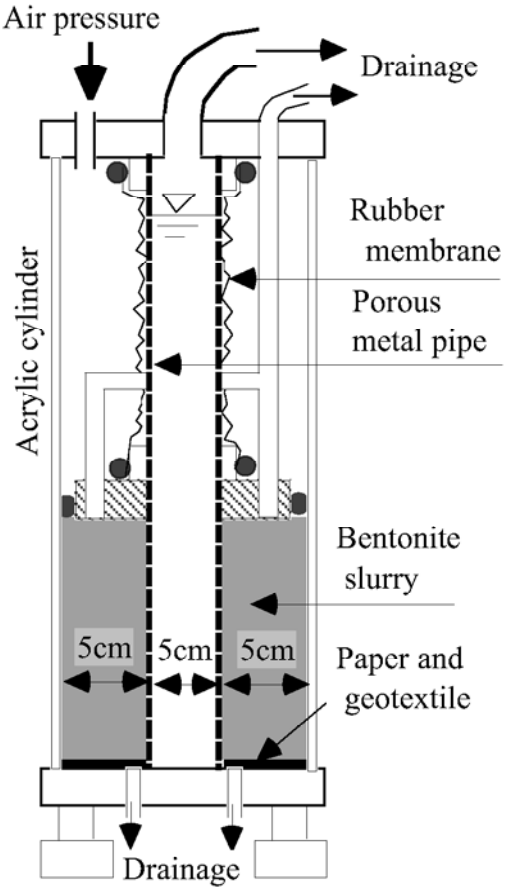

Fig. 10.67 Consolidation tank for preparation of hollow cylindrical specimen of water-saturated bentonite (Nakamura et al., 2007)

Fig. 10.68 Appearance of bentonite specimen after preconsolidation under 98 kPa

the damping ratio is lower. Thus, more plastic soils have less extent of nonlinearity as stated in Sect. 10.2.

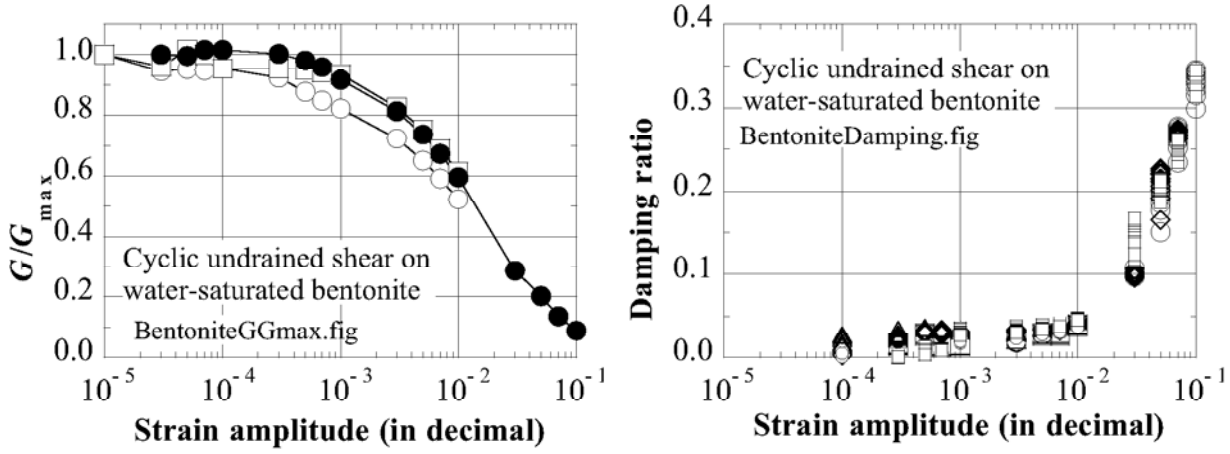

Fig. 10.69 Variation of $G/G_{\max}$ and damping ratio of water-saturated Na-bentonite

10.24 Nonlinear Cyclic Behavior of Municipal Solid Waste

A recent target of geotechnical engineering is a landfill that is composed of municipal solid waste. In principle, there are three kinds of waste, which are unprocessed wastes, incinerated ash, and incombustible wastes, that are composed of plastics, metals, soil, ceramics, etc. Such unprocessed wastes as food and other organic materials are either damped directly in landfills to be subjected to bio-disintegration or incinerated (burnt) to be ash. Figure 10.70 shows a landfill in Delaware of USA where wastes are directly damped. Figure 10.71 is indicative of an incinerated ash ground near Tokyo. The appearance of this material is similar to sand. Figure 10.72 reveals a damping site of plastic wastes. The original plastics are shredded into small pieces prior to damping. It is important that the incombustible wastes include organic waste as well because of the inclusion of unfinished lunch boxes etc. In many municipalities, organic and incombustible wastes are separated in families prior to damping. In contrast, a recent technology has made it possible to incinerate all the family wastes under higher temperatures, and the produced slug waste looks similar to clean gravel (Fig. 10.73).

Fig. 10.70 Unprocessed waste landfill in Willmington of Delaware

Fig. 10.71 Trench cut in landfill of incinerated ash in Tokyo

Fig. 10.72 Landfill of plastic waste in Tokyo

Fig. 10.73 Landfill of incinerated slugs in Yokohama

Many people imagine that municipal waste is a very soft and unstable material. This idea is supported by failure accidents of landfills such as the Payatas landfill near Manila, the Philippines, in 2000 (Merry et al. 2005), and another one in Bandung of Indonesia (2005, Fig. 10.74). Most of these failures were induced by heavy rainfalls and the lack of compaction of the waste. Vincential Missionaries (1998) reported the pre-failure situation of the Payatas landfill. There are, however, examples in which nearly vertical cliffs of municipal waste have been stable for many years (Figs. 10.75 and 10.76). As is clearly seen in Fig. 10.75, these stable cliffs are stabilized by such fibrous materials as paper, clothes, strings, etc. This stabilizing mechanism is identical with those employed in modern reinforced soils. Noteworthy

is that the reinforcement by fibers is destroyed by fires, making the landfill less unstable. Both Payatas and Bandung landfills had fire prior to failure (Merry et al. 2005, Kölsch et al. 2005).

A series of triaxial drained compression tests were conducted on bio-treated waste that was collected at the Yever landfill near Wilhelmshafen, Germany (Fig. 10.77) (Towhata et al. 2004 and Itoh et al. 2005). Figure 10.78 illustrates test results. It is interesting that tested samples revealed approximately linear stress–strain relationships and did not yield within the range of the test (within the strain capacity of a triaxial device). By comparing these results with the behavior of densified Toyoura sand in the same figure, it may be said that the tested waste has better shear resistance. The deformation modulus of waste is, on the contrary, much lower than that of sand, implying that waste is significantly softer than sand.

Fig. 10.74 Failure of Leuwigajah landfill near Bandung, Indonesia

Fig. 10.75 Vertical and stable cliff in landfill near Göttingen, Germany

Fig. 10.76 Stable waste cliff in Tokyo (Photo by Y. Imai)

Fig. 10.77 Ongoing field bio-treatment in Yever landfill in Germany

An important feature in Fig. 10.78 is the behavior of the organic waste from which the reinforcing fibrous materials were removed. As expected, the stress–strain curve reveals yielding followed by softening of the stress level. Note further that the incombustible waste from Tokyo site is extremely soft, but still exhibits stress level higher than that of sand in a large strain range.

More recently, a large triaxial shear device was constructed for waste tests (Towhata et al. 2007). Since the grain size of incombustible waste reaches several centimeters, at maximum, a specimen size of 30 cm in diameter and 60 cm in height was considered necessary. After obtaining approximately linear stress–strain behavior (similar to Fig. 10.78), cyclic triaxial tests were conducted to measure shear modulus and damping ratio of Tokyo's incombustible waste (Fig. 10.79). In this study, shear stress and shear strain were defined by

$$\tau \equiv (\sigma_a - \sigma_r)/2 \text{ and } \gamma \equiv \varepsilon_a - \varepsilon_r$$

by using triaxial stress and strain data.

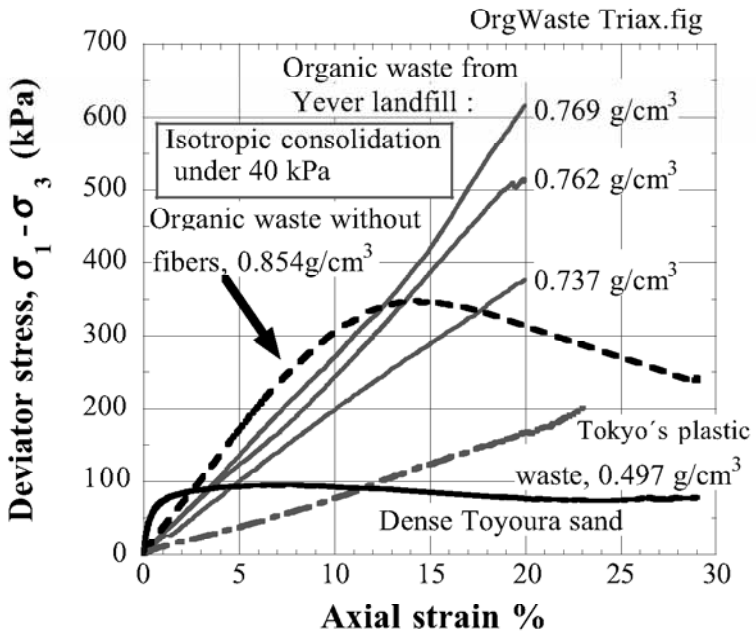

Fig. 10.78 Triaxial shear tests on waste

Fig. 10.79 Incombustible waste collected from Tokyo landfill

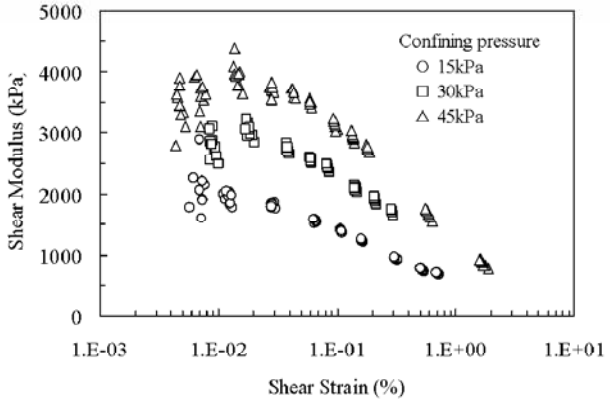

Fig. 10.80 Variation of shear modulus of Tokyo incombustible waste with strain amplitude

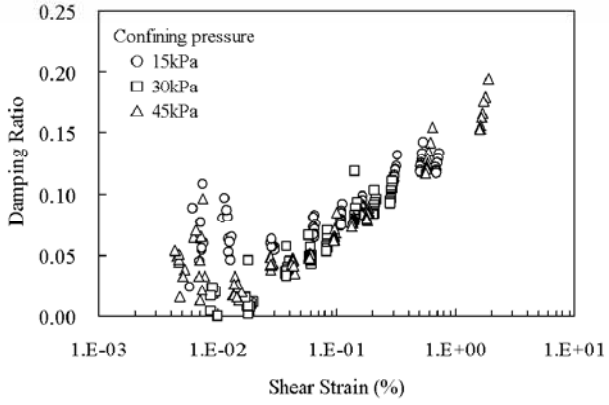

Fig. 10.81 Variation of damping ratio of Tokyo incombustible waste with strain amplitude

Figures 10.80 and 10.81 illustrate the nonlinear properties of incombustible waste. Although there is some uncertainty in the strain range of 0.01% or less (due probably to large grain size), the nonlinearity in the greater strain range is consistent with what have been known on other soils. The values of shear modulus (Fig. 10.80) is somewhat lower than modulus of soils under similar stress. Thus, the natural period of a landfill of incombustible wastes is longer than in soil deposits.

Incinerated ash appears similar to gravelly sand (Fig. 10.82). It is important that this ash reacts with water and gains intergranular bonding; Fig. 10.83 shows that surface of grains are covered by cementing materials after water submergence. Consequently, a deposit of incinerated ash comes to exhibit a very high rigidity. Figure 10.84 illustrates the results of a triaxial compression test in which loading was paused for 1–6 h after large strain. It is evident that the stress level increased while loading stopped and the mechanical damage (yielding) during previous loading was cured in the meantime (self curing).

Fig. 10.82 Incinerated ash collected from Tokyo Bay landfill

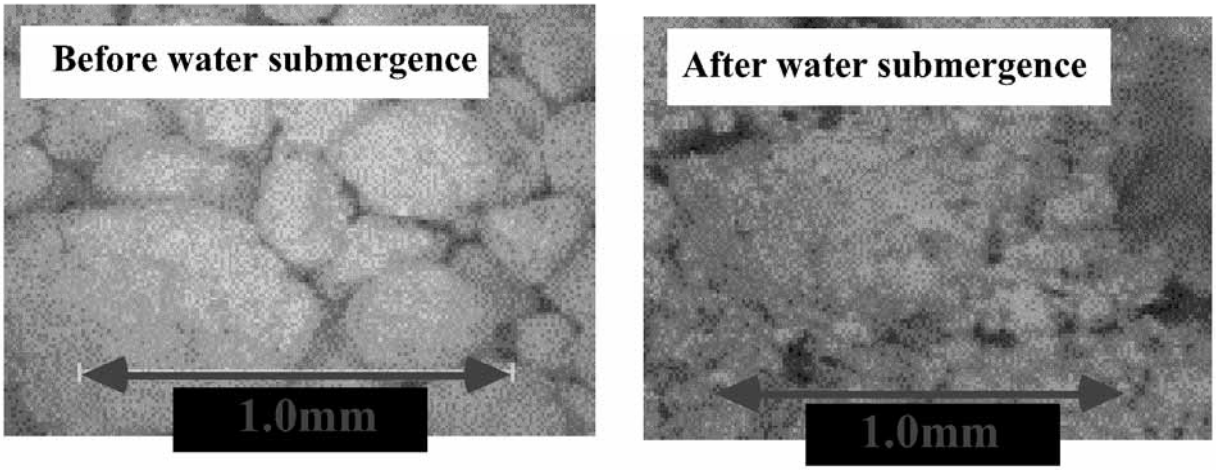

Fig. 10.83 Appearance of incinerated ash before and after water submergence

The cyclic properties of incinerated ash were studied by torsion shear tests. Figures 10.85 and 10.86 demonstrate that the modulus becomes small at a strain of 10% (0.1). The significant increase in damping ratio beyond this strain value may be due to shear failure. In general, the behavior of incinerated ash is similar to what have been know for other soils.

As may be known, one of the significant problems in municipal waste landfill is the long-term consolidation. Uno et al. (2007) found experimentally that this problem can be solved by preloading in which the stress level in landfill is temporarily increased by additional soil filling and, after several months when substantial subsidence has occurred, the soil is removed.

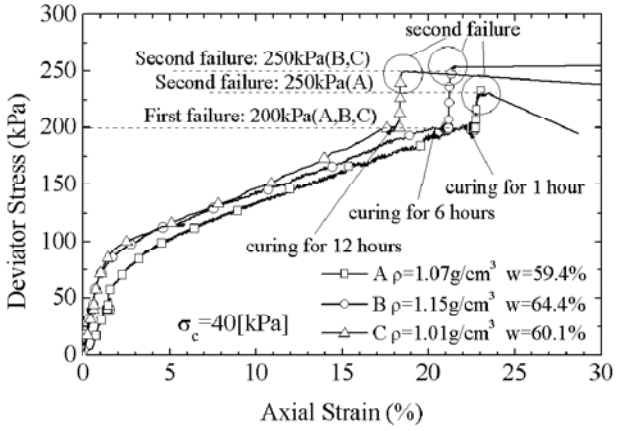

Fig. 10.84 Development of cementation and its effect on stress–strain behavior of incinerated ash

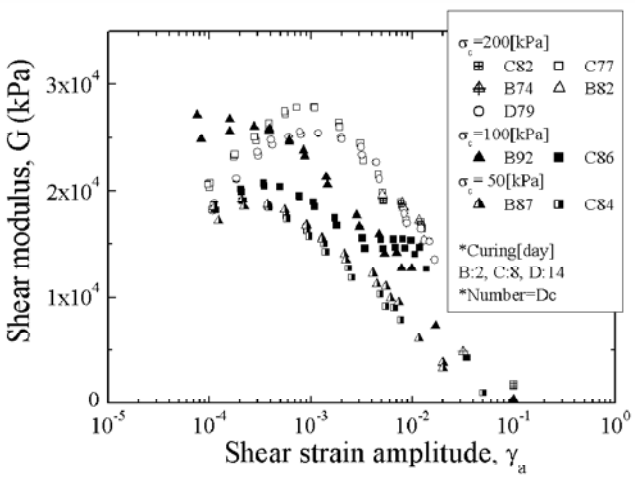

Fig. 10.85 Variation of shear modulus of incinerated ash with shear strain amplitude

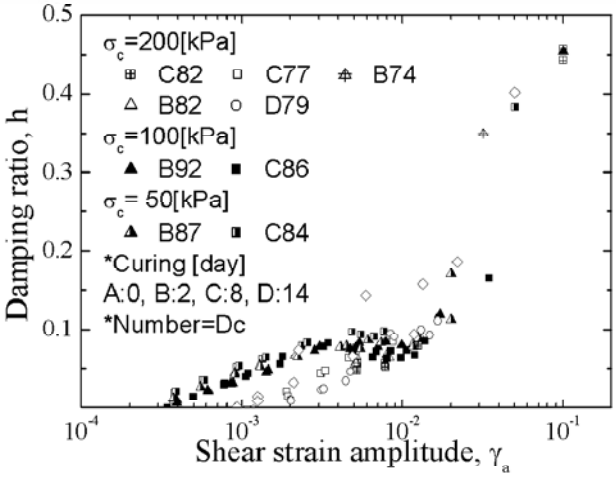

Fig. 10.86 Variation of damping ratio of incinerated ash with shear strain amplitude

List of References in Chapter 9

Afifi, S.S. and Richart Jr., F.E. (1973) Stress-history effects on shear modulus of soils, Soils Found., Vol. 13, No. 1, pp. 77–95.

Anderson, D.G. and Woods, R.D. (1976) Time–dependent increase in shear modulus of clay, J. Geotech. Eng., ASCE, Vol. 102, pp. 525–537.

Brignoli, E.G.M., Gotti, M. and Stokoe, K.H.I. (1996) Measurement of shear waves in laboratory specimens by means of piezoelectric transducers, Geotech. Test. J., Vol. 19, No. 4, pp. 384–397.

Casagrande, A. and Shannon, W.L. (1948a) Research on stress-deformation and strength characteristics of soils and rocks under transient loading, Harvard University Soil Mechanics Series, No. 31.

Casagrande, A. and Shannon, W.L. (1948b) Strength of soils under dynamic loads, Proc. ASCE, Vol. 74, No. 4, pp. 591–608.

Chijimatsu, M., Fujita, T., Suzuki, H. and Matsumoto, K. (1999) Hydraulic properties of buffer material, Bulletin of Japan Nuclear Cycle Development Institute, No. 5.

Chung, R.M., Yokel, F.Y. and Drnevich, V.P. (1984) Evaluation of dynamic properties of sands by resonant column testing, Geotech. Test. J., Vol. 7, No. 2, pp. 60–69.

Dobry, R. and Vucetic, M. (1987) Dynamic properties and seismic response of soft clay deposits, Proc. Intern. Symp. Geotech. Eng. Soft Soils, Vol. 2, pp. 51–87.

Ellis, E.A., Soga, K., Bransby, M.F. and Sato, M. (2000) Resonant column testing of sands with different viscosity pore fluids, J. Geotech. Geoenviron. Eng., ASCE, Vol. 126, No. 4, pp. 10–17.

Fujiwara, T., Horikoshi, K. and Sakai, K. (2005) Development of a sampler designed for laminar box and its application to dynamic centrifuge modeling of footing settlement due to liquefaction, Proc. 16th Int. Conf. Soil Mech. Geotech. Eng., Vol. 4, pp. 2645–2648.

Goto, S., Tatsuoka, F., Shibuya, S., Kim, Y.S. and Sato, T. (1991) A simple gauge for local small strain measurements in the laboratory, Soil Found., Vol. 31, No. 1, pp. 169–180.

Hara, A. (1973) Dynamic nature of ground and its application in practice 地盤の動力学的性質とその応用, Proc. 2nd Symp. on Dynamic Behavior of Ground 第２回地盤振動シンポジウム, AIJ 建築学会, pp. 33–39 (in Japanese).

Hardin, B.O. (1978) The nature of stress–strain behavior for soils, ASCE Geotech. Engg. Div. Specialty Conf. Earthq. Eng. Soil Dynam., Vol. I, pp. 3–90.

Hardin, B.O. and Black, W.L. (1968) Vibration modulus of normally consolidated clay, Proc. ASCE, Vol. 94, SM2, pp. 353–369.

Hatanaka, M., Uchida, A. and Oh-oka, H. (1995) Correlation between the liquefaction strengths of saturated sands obtained by in-situ freezing method and rotary-type triple tube method, Soils Found., Vol. 35, No. 2, pp. 67-75.

Humphries, W.K. and Wahls, H.E. (1968) Stress history effects on dynamic modulus of clay, Proc. ASCE, Vol. 94, SM2, pp. 371–389.
Idriss, I.M., Dobry, R. and Singh, R.D. (1978) Nonlinear behaviour of soft clays during cyclic loading, Proc. ASCE, Vol. 104, GT12, pp. 1427–1447.
Iida, K. (1938) The velocity of elastic waves in sand, Bulletin of Earthquake Research Institute, University of Tokyo, Vol. 16, pp. 131–145.
Imazu, M. and Fukutake, K. (1986) Dynamic shear modulus and damping ratio of gravel materials, Proc. 21st Annual Convention of JSSMFE, pp. 509–512.
Ishimoto, M. and Iida, K. (1936) Determination of elastic constants of soils by means of vibration methods, Part 1. Young's modulus, Bulletin of Earthquake Research Institute, University of Tokyo, Vol. 14, pp. 632–657.
Ishimoto, M. and Iida, K. (1937) Determination of elastic constants of soils by means of vibration methods, Part 2. Modulus of rigidity and Poisson's ratio, Bulletin of Earthquake Research Institute, University of Tokyo, Vol. 15, pp. 67–85.
Itoh, T., Towhata, I., Kawano, Y., Kameda, M., Fukui, S., Kölsch, F. and Yonai, Y. (2005) Mechanical properties of municipal waste deposits and ground improvement, Proc. XVIth International Conference on Soil Mechanics and Geotechnical Engineering, Osaka Vol. 4, pp. 2273–2276.
Japanese Geotechnical Society (1995) Field soil investigation, p. 154 and p. 164 (in Japanese).
Kölsch, F., Fricke, K., Mahler, C. and Damanhuri, E. (2005) Stability of landfills – The Bandung dumpsite disaster, Proceedings of the 10th Int. Landfill Symposium, Cagliari.
Kokusho, T. (1982) Dynamic deformation characteristics of soils and nonlinear seismic response of ground, Doctoral Thesis, University of Tokyo (in Japanese).
Kokusho, T. (1982) Dynamic soil properties and nonlinear seismic response of ground, Doctoral Thesis, University of Tokyo (in Japanese).
Kokusho, T., Yoshida, Y. and Esashi, Y. (1982) Dynamic properties of soft clay for wide strain range, Soil Found., Vol. 22, No. 4, pp. 1–18.
Kokusho, T. (1987) In-situ dynamic soil properties and their evaluations, Proc. 8th Asian Regional Conf. Soil Mech. Found. Engg., Vol. 2, pp. 215–240.
Lefebvre, G. and Pfendler, P. (1996) Strain rate and preshear effects in cyclic resistance of soft clay, J. Geotech. Geoenviron. Eng., ASCE, Vol. 122, No. 1, pp. 21–26.
Lefebvre, G. and LeBoeuf, D. (1987) Rate effects and cyclic loading of sensitive clays, J. Geotech. Eng., ASCE, Vol. 113, No. 5, pp. 476–489.
Maqbool, S. and Koseki, J. (2006) Effects of compaction on dynamically and statically measured small strain stiffness of gravel, Proceedings of International Conference on Earthquake Engineering (ICEE), Lahore, Pakistan, pp. 161–175.
Marcuson III, W.F. and Wahls, H.E (1978) Effects of time on damping ratio of clays, ASTM STP 654 Dynamic Geotechnical Testing, pp. 126–147.
Merry, S.M., Kavazanjian, E. and Fritz, W.U. (2005) Reconnaissance of the July 10, 2000, Payatas Landfill Failure, J. Performance Construct. Facilities, ASCE, Vol. 19, No. 2, pp. 100–107.
Mesri, G. and Olson, R.E. (1970) Shear strength of montmorillonite, Geotechnique, Vol. 20, No. 3, pp. 261–270.
Nakamura, M., Thuan, B.T., Uchimura, T., Sugo, K. and Towhata, I. (2007) Torsional shear tests on water-saturated bentonite samples and method of sample preparation, to be submitted to Soils and Foundations.
Olson, R.E. (1974) Shearing strengths of kaolinite, illite and montmorillonite, Proc. ASCE, Vol. 100, GT11, pp. 1215–1229.
Osipov, V.I., Gratchev, I.B. and Sassa, K. (2005) The mechanism of liquefaction of clayey soils (M124), Chap. 15, Landslides: Risk Analysis and Sustainable Disaster Management, pp. 127–131, Springer, Berlin, Heidelberg, New York.
Richart Jr., F.E., Hall, J.R. and Woods, R.D. (1970) Vibrations of soils and foundations, Prentice-Hall, Japanese translation : 土と基礎の振動、岩崎・嶋津訳、鹿島出版会.
Tanaka, Y., Kudo, K., Nishi, K., Okamoto, T., Kataoka, T. and Ueshima, T. (2000) Small strain

characteristics of soils in Hualien, Taiwan, Soils Found., Vol. 40, No. 3, pp. 111–125.
Tani, K. and Kaneko, S. (2006) Undisturbed sampling method using thick waste-soluble polymer solution, Tsuchi-to-Kiso: Monthly Magazine of Japan. Geotech. Soc., Vol. 54, No. 4, pp. 19-21 (in Japanese).
Tokimatsu, K. (1995) Quality of undisturbed samples, Field soil investigation, Japanese Geotechnical Society, p. 150.
Tokimatsu,K., Midorikawa, S. and Yoshimi,Y. (1989) Dynamic soil properties obtained from strong motion records, Proc. 12th Int. Conf. Soil Mech. Found. Eng., Vol. 3, pp. 2015-2018.
Towhata, I., Haga, K. and Nakamura, S. (1985) Effects of cyclic drained shear or rigidity of sand, Proc. 20th Nat. Conf. Soil Mech. Found. Eng., Vol. 1, pp. 591–592.
Towhata, I., Kawano, Y., Yonai, Y. and Kölsch, F. (2004) Laboratory tests on dynamic properties of municipal waste, Proc. the 11th Int. Conf Soil Dynamics and Earthquake Engineering and the 3rd International Conference on Earthquake Geotechnical Engineering, Berkeley, Vol. 1, pp. 688–693.
Towhata, I., Uno, M., Kawano, Y., Kameda, M., Kita, Y. and Yonai, Y. (2007) Laboratory tests on mechanical properties of municipal waste solid waste, to be submitted to Proc. JSCE (in Japanese).
Uno, M., Itoh, T., Imai, Y., Tsujimura, T., Towhata, I., Fukui, S., Kita, Y. and Watanabe, Y. (2007) Laboratory tests on improvement of mechanical properties of municipal solid waste, to be submitted to Proc. JSCE (in Japanese).
Viggiani, J. and Atkinson, J.H. (1995) Interpretation of bender element tests. Geotech., Vol. 45, No. 1, pp. 149–154.
Vincentian Missionaries (1998) The Payatas environment programme: micro-enterprise promotion and involvement in solid waste management in Quezon City, Environment and Urbanization, Vol. 10, No. 2, pp. 55–68.
Yasuda, S. and Yamaguchi, I. (1984) Dynamic shear modulus of sand obtained from laboratory and in-situ tests, Symp. Monitoring Deformation and Strength of Sand and Sandy Ground, JSSMFE, pp. 115–118.
Yasuda, S. and Yamaguchi, I. (1985) Dynamic soil properties of undisturbed samples, 20th Ann. Conv. JSSMFE, pp. 539–542, Nagoya.
Yoshimi, Y. and Goto, S. (1996) Liquefaction resistance of silty sand based on in situ frozen samples, Geotech., Vol. 46, pp. 153–156.
Yoshimi, Y., Hatanaka, M., Oh-Oka, H. and Makihara, Y. (1985) Liquefaction of sands sampled by in situ freezing, Proc. 11th ICSMFE, Vol. 4, pp. 1927–1930.
Yoshimi, Y., Tokimatsu, K. and Ohara, J. (1994) In situ liquefaction resistance of clean sands over a wide density range, Geotech., Vol. 44, No. 3, pp. 479–494.